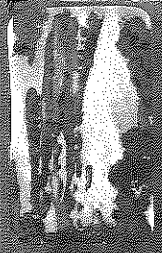

A-38

HEAT FLOW AND MICROEARTHQUAKE STUDIES, COSO GEOTHERMAL AREA, CHINA LAKE, CALIFORNIA FINAL REPORT

July, 1975

Jim Combs

HEAT FLOW AND MICROEARTHQUAKE STUDIES, COSO GEOTHERMAL AREA

CHINA LAKE, CALIFORNIA

FINAL REPORT

JULY, 1975

Jim Combs

Institute for Geosciences
The University of Texas at Dallas
P. O. Box 688 Station FO 21
Richardson, Texas 75080

Contract No.	N00123-74-C-2099
Program Code	4F10
Effective Date	1 June 1974
Expiration Date	31 May 1975
Amount of Contract	$97,716

Sponsored by
Advanced Research Projects Agency
ARPA Order No. 2800

CONTENTS

Figures:

Tables:

HEAT FLOW AND MICROEARTHQUAKE STUDIES, COSO GEOTHERMAL AREA, CHINA LAKE, CALIFORNIA

Final Report

ABSTRACT

The present research effort at the Coso Geothermal Area located on the China Lake Naval Weapons Center, China Lake, California, was concerned with: (1) heat flow studies and (2) microearthquake studies associated with the geothermal phenomena in the Coso Hot Springs area. The sites for ten heat flow boreholes were located primarily using the available seismic ground noise and electrical resistivity data. Difficulty was encountered in the drilling of all of the holes due to altered, porous, faulted, and sometimes highly fractured zones. Thermal conductivity measurements were completed using both the needle probe technique and the divided bar apparatus with a cell arrangement. Heat flow values were obtained by combining equilibrium temperature measurements with the appropriate thermal conductivity values. Heat, in the upper few hundred meters of the subsurface associated with the Coso Geothermal Area, is being transferred by a conductive heat transfer mechanism with a value of approximately 15 $\mu cal/cm^2$-sec. This is typical of geothermal systems throughout the world and is approximately ten times the normal terrestrial heat flow of 1.5 HFU. The background heat flow for the Coso region is about 3.5 HFU.

During the summer of 1974, two different arrays of portable high-gain seismographs were installed in the Coso Geothermal Area. The first array consisted of six vertical-component, smoked paper drum recorders, while the second consisted of nine, three-component, magnetic tape recorders. Over the period

of recording, the microearthquake activity changed considerably including days which had only a few events while others had as many as 100 or more distinct local events. During thirty-three days of recording, more than two thousand events with S-P times of less than three seconds were detected. Strain release in the Coso Geothermal Area occurs primarily in swarm-type sequences whereas earthquakes outside the area occur as mainshock-aftershock sequences.

Detailed subsurface velocity data, obtained from 9 calibration blasts, indicate an essentially constant P-wave velocity of 4.75 km/sec for the upper 5 km overlying a half space of 6.0 km/sec, which is in excellent agreement with previous refraction studies in the region. Hypocenters are predominately between 1 and 6 km with an increase in focal depth from the Coso Hot Springs toward the west and northwest. Areas of high seismic noise outlined in an earlier survey tend to coincide with areas of high microearthquake activity with an additional inverse correlation between the focal depth and amplitude of the noise.

Using a reduced Wadati diagram and a least squares linear regression analysis, we obtained a value of 1.57 for the ratio of V_P to V_S compared to values of 1.73 to 1.87 usually obtained in laboratory and field investigations. We calculated an S-wave velocity of 3.03 km/sec. These P- and S-wave velocities infer a Poisson's ratio of 0.16 compared with the values of 0.25 to 0.30 which are normally observed. The low value for Poisson's ratio observed for the Coso Geothermal Area indicates that the shallow subsurface is either deficient in liquid water saturation or more likely that the void spaces (cracks) are filled with steam. These data indicate that the Coso geothermal system is a vapor-dominated system rather than a hot-water system. The Coso Geothermal Area appears to have the potential for production of hot brines from shallow zones, for production of dry steam, and for areas of hot dry rock.

INTRODUCTION

The Coso Geothermal Area, located primarily on the China Lake Naval Weapons Center in Inyo County, California (Fig. 1), is situated in a tectonically active area (Hileman, et al., 1973) of young basaltic and rhyolitic volcanism (Evernden, et al., 1964; Lanphere, et al., 1975; Duffield, 1975). Hot springs and fumaroles associated with the young volcanism have been known for years; consequently, the area has been classified as a Known Geothermal Resources Area, KGRA (Godwin, et al., 1971). The Coso Geothermal Area is of considerable interest for the exploration and development of geothermal resources.

Several geological as well as surface and airborne geophysical techniques (Frazer, et al., 1943; Austin and Pringle, 1970; Austin, et al., 1971; Koenig, et al., 1972; Teledyne Geotech, 1972; Furgerson, 1973; Lanphere, et al., 1975; Duffield, 1975) have been used in the Coso Geothermal Area in order to detect and to initially determine the extent and potential of this geothermal system. Most of the available data can provide some guidance for the selection of a site for an exploratory geothermal drill hole. Until now, however, the one geophysical technique, that is, heat flow measurements, that can indicate the presence or absence of abnormal heat has not been utilized.

Investigations of microearthquake activity associated with geothermal resources in some tectonically active areas as well as volcanic areas have shown that occurrences of these resources are often characterized by a relatively high level of such activity (Westphal and Lange, 1962; Brune and Allen, 1967; Lange and Westphal, 1969; Ward, et al., 1969; Ward and Björnsson, 1971; Ward and Jacob, 1971; Hamilton and Muffler, 1972; Ward, 1972; Combs and Hadley, 1976).

The objectives of these reconnaissance studies were to determine the magnitude of the heat flux and to determine the background level of seismic activity

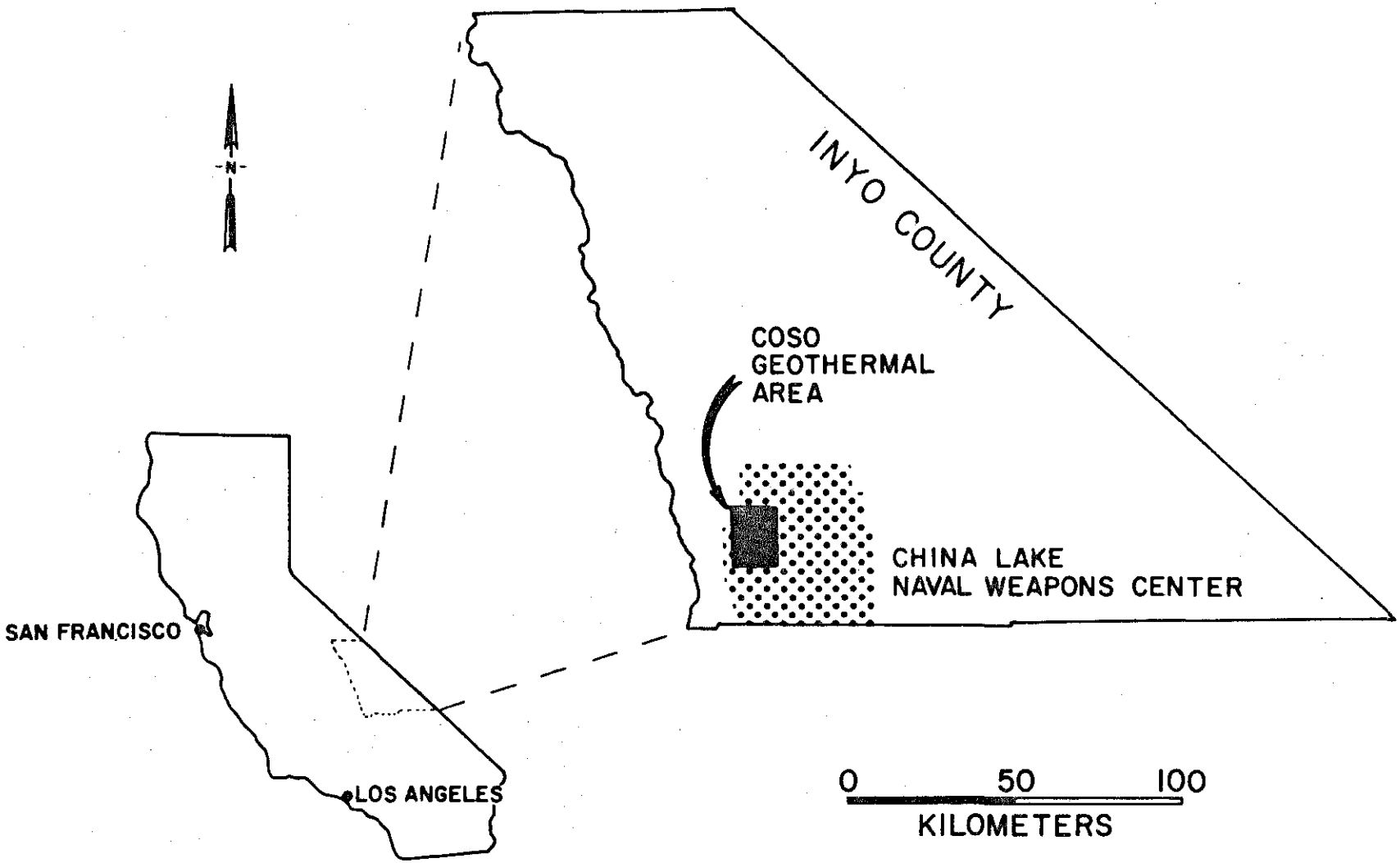

Figure 1. Location map of the Coso Geothermal Area, California. Shaded rectangle depicts area of the microearthquake investigation.

associated with the Coso Geothermal Area prior to the onset of potential effects caused by future drilling, production, and reinjection of fluids into the presumed geothermal reservoir. In addition, from the study of microearthquakes and their precise hypocentral locations, it will be possible to determine any active fault zones in the area which may be functioning as subsurface conduits for the presumed geothermal reservoir. Finally, the present heat flow and microearthquake surveys will be used to speculate on the subsurface physical characteristics of the Coso geothermal system.

GEOLOGICAL AND GEOPHYSICAL BACKGROUND

The geologic setting of the Coso Geothermal Area consists of Mesozoic granitic and metamorphic rocks overlain by upper Cenozoic volcanic rocks and shallow Quaternary alluvial deposits in the scattered, small basins (Koenig, et al., 1972; Duffield, 1975). Rhyolite domes and rhyolitic and basaltic lava flows which range in age from 0.04 to 0.96 m.y. with most of the units ranging in age from 0.05 to 0.15 m.y. occur on a north trending structural and topographic high (Evernden, et al., 1964; Lanphere, et al., 1975).

The area has been extensively faulted with the Coso Mountains broken into a pattern of roughly north to northeast and northwest trending, steeply dipping faults. The geothermal area is characterized by arcuate fractures with radially trending fractures to these arcuate zones (Austin, et al., 1971; Koenig, et al., 1972). From a detailed study of the volcanism and structural relations of the region, Duffield (1975) has suggested that all of the volcanic rocks are encompassed by an oval-shaped zone of late Cenozoic ring faulting that has dimensions of about 45 km east-west and 35 km north-south defining a structural basin (Fig. 2). The ring structure and associated young volcanic rocks imply a caldera-like feature caused by uplift and fracture accompanied by extrusions and surficial subsidence. In other words, a large underlying magma chamber that appears to have periodically erupted lava to the surface during the past few million years and to have resulted in the present geothermal phenomena.

Fumaroles and hot springs are situated at scattered locations throughout the Coso Geothermal Area. Although the geothermal activity in the form of fumarolic and hot springs activity has been known for many years (Frazer, et al., 1943), the geothermal manifestations were not studied in detail until the late 1960's (Austin and Pringle, 1970). A combination of field geological reconnaissance,

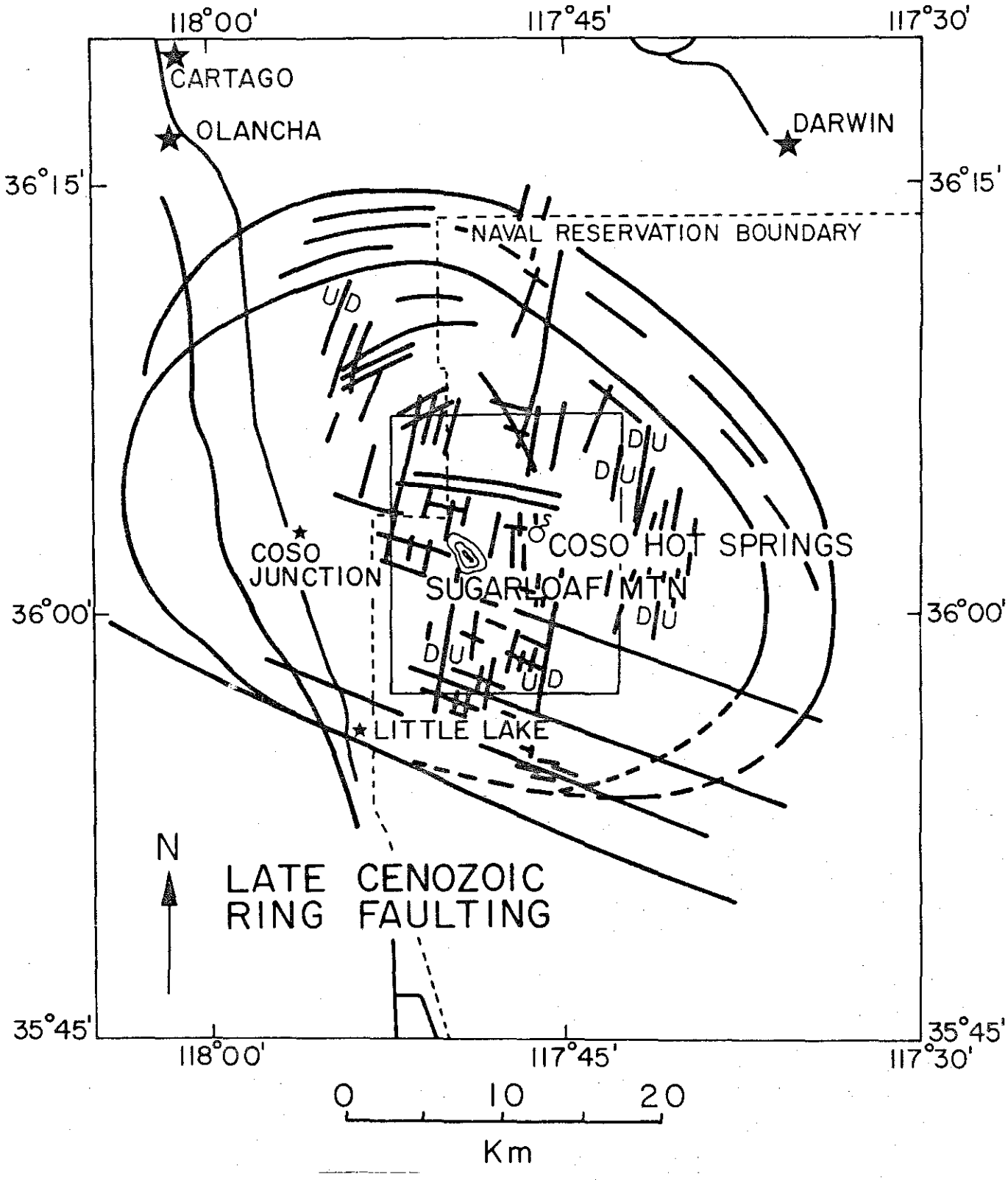

Figure 2. Sketch map of the faults in the Coso Geothermal Area (modified from Duffield, 1975). Inner rectangle denotes extent of present study area.

photogeology, theoretical petrology, gravity and magnetometer measurements, and mineralogical investigations culminated in 1967 with the drilling of the Coso No. 1 drill hole into the thermally active Coso Fault Zone adjacent to the Coso Hot Springs (Austin and Pringle, 1970). The hole was drilled to 114 m and has a maximum temperature of 142°C.

Several surface and airborne geophysical techniques have been used in order to detect and to initially determine the potential and extent of any geothermal systems in the Coso Hot Springs area. Koenig, et al., (1972) noted that color photography and snowmelt patterns (White, 1969) were of greatest utility in locating areas of presently active thermal fluid leakage. Infrared imagery appeared to be of value in delineating the arcuate structural patterns associated with the geothermal deposits (Koenig, et al., 1972).

A detailed geothermal seismic noise survey was completed by Teledyne Geotech (1972). The results of the noise survey of the Coso Geothermal Area clearly show the presence of high noise levels with three separate high frequency anomalies (Fig. 3). The largest of these anomalies with the highest amplitude is associated with the Coso Hot Springs. Of the two other anomalies, one is close to the fumarolic area known as Devil's Kitchen, while the third is not connected with known surface activity. These data imply a correlation between geothermal phenomena and high seismic noise level.

The geothermal noise survey was followed by a total field DC resistivity investigation (Furgerson, 1973). The granitic host rock has an apparent resistivity of 200 ohm-m or more, whereas the surface thermal manifestations appear to have resistivities below 50 ohm-m (Fig. 4). Thus, from the results of the roving dipole technique there seems to be a contrast in apparent resistivities by a

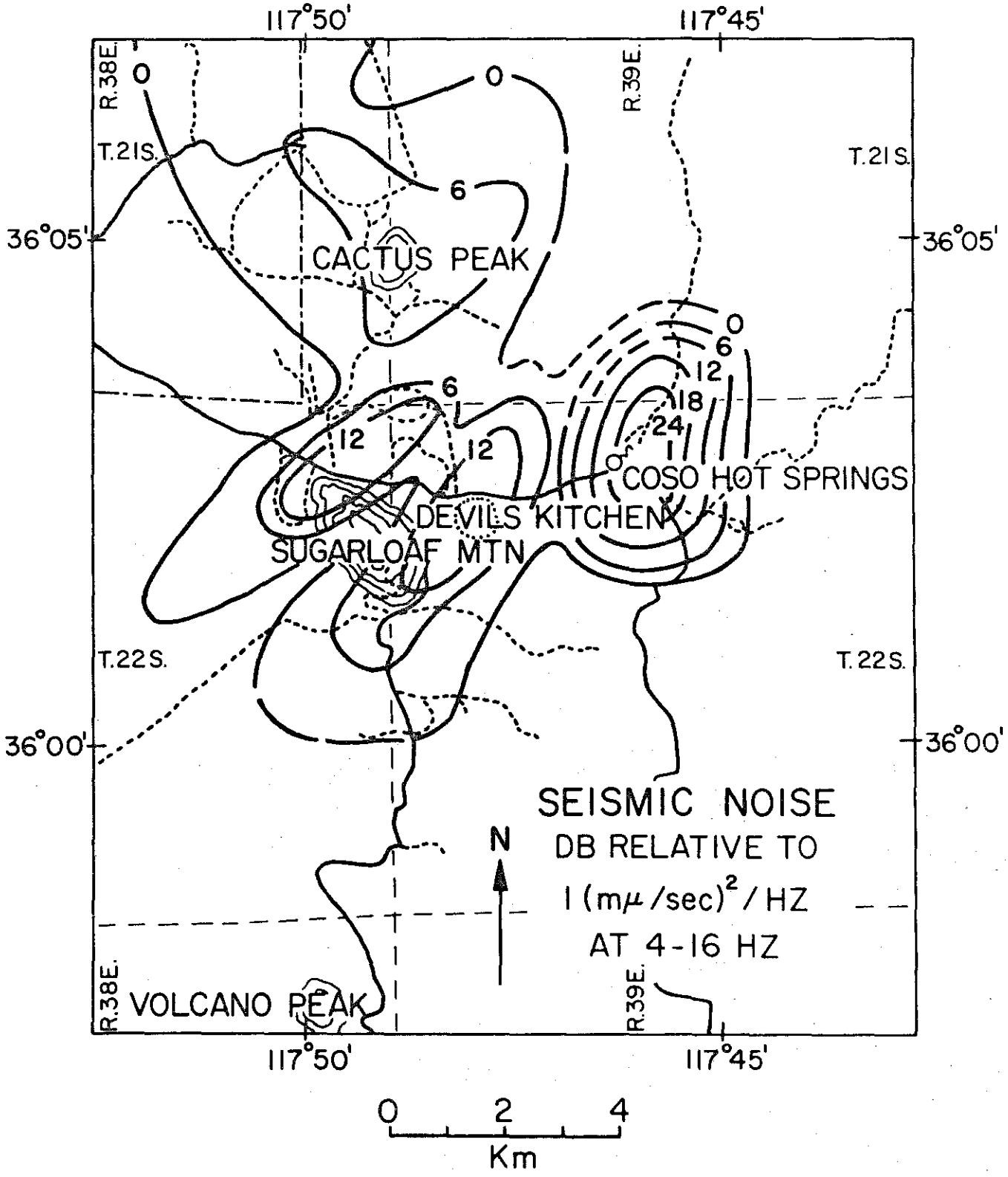

Figure 3. Seismic ground noise map of the Coso Geothermal Area. Contours are given in decibels relative to 1 (millimicron/sec)^2 per Hertz in the pass band of 4 to 16 Hz (modified from Teledyne Geotech, 1972).

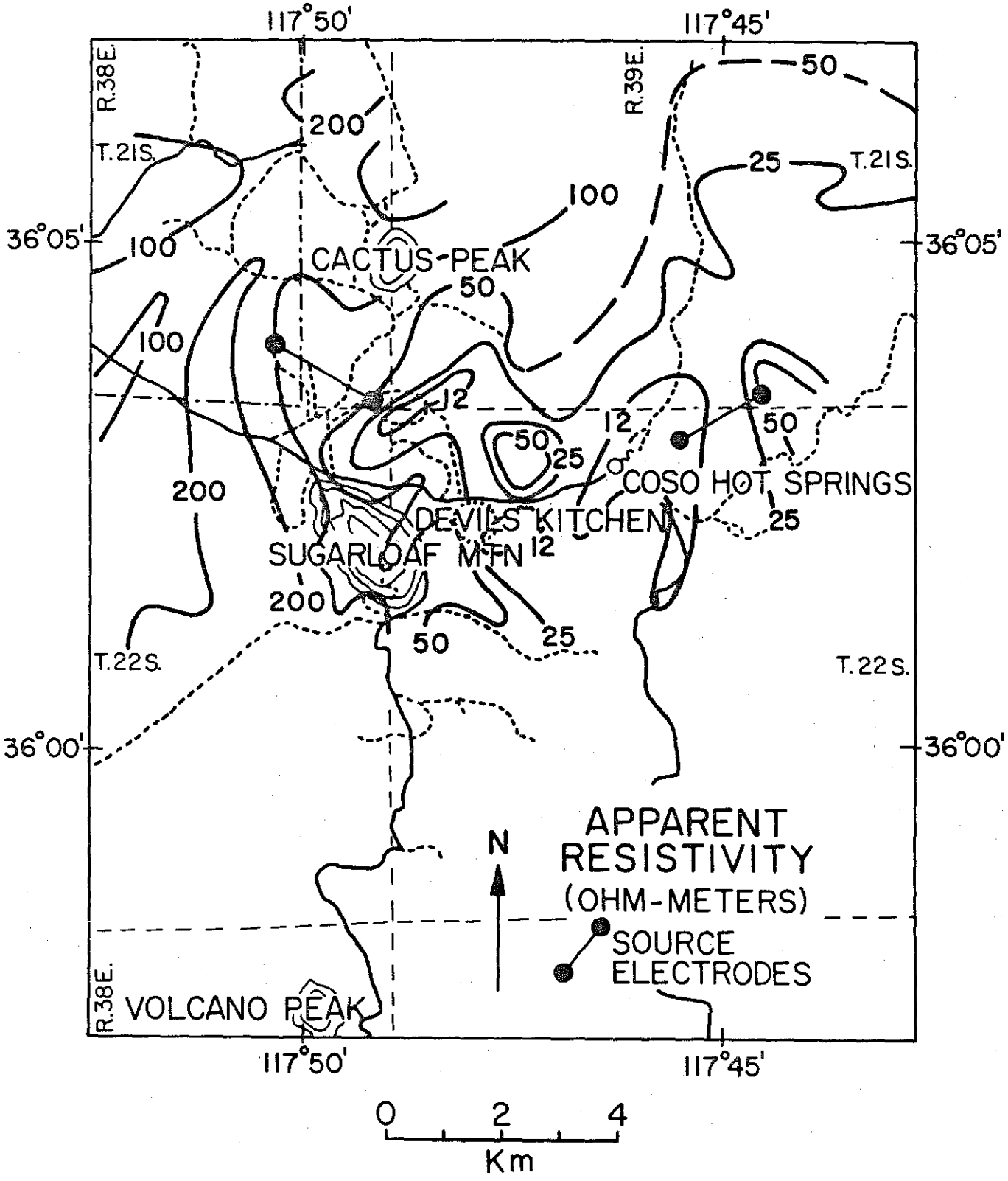

Figure 4. Total field apparent resistivity map of the Coso Geothermal Area. The minimum apparent resistivity in ohm-meters for the two source dipoles is contoured (modified from Fig. 21, Furgerson, 1973).

factor of about 10 between the normal and the geothermally effected regions. The dipole maps may be used in locating or extending some of the faults and/or the fractures which appear to control at least the surface geothermal activity and probably the deeper plumbing of the presumed geothermal reservoir.

The Coso Geothermal Area is tectonically active, manifested in frequent earthquakes, as indicated by the pattern of regional seismicity shown in Figure 5. Epicenters from the California Institute of Technology seismograph network for the period 1953 to 1972 are plotted in Figure 5 (Hileman, et al., 1973). These earthquakes are of magnitude 3 or greater. Events appear to occur outside of the immediate area of the geothermal activity as may be noted in the area demarcated by a rectangle in Figure 5 which is the area of the present investigation.

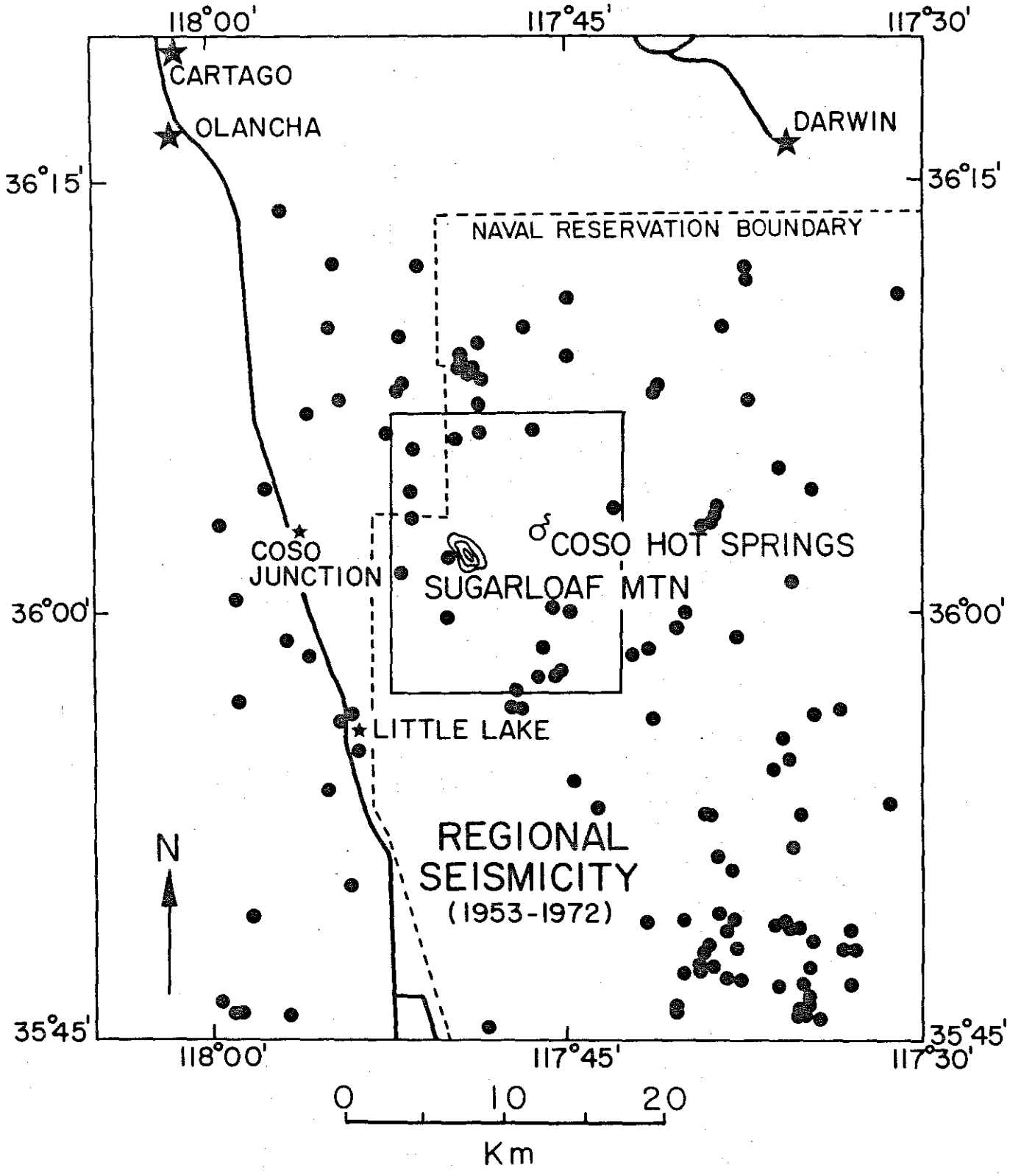

Figure 5. Regional seismicity as indicated by the epicenters for earthquakes of magnitude $\geq$ 3, located by the California Institute of Technology Seismological Network, 1953-1972 (modified from Hileman, et al., 1973).

HEAT FLOW INSTRUMENTATION AND FIELD PROCEDURE

Determination of the terrestrial heat flow requires the measurement of two different quantities, specifically, the geothermal gradient and the thermal conductivity of rocks in which the gradient has been obtained. Estimation of heat flow therefore requires the drilling of boreholes, the determination of the thermal conductivity of the strata penetrated and finally measurement of the temperature gradient across these strata.

Drilling was completed on all ten heat flow boreholes (Table 1) that were selected. Difficulty was encountered in all of the holes. Only one of the sites, UTD-Coso #6, reached the originally specified depth of 92 meters. Altered, porous, faulted, fractured, and sometimes poorly consolidated zones were encountered which hampered drilling with the compressed air drill rig. Boreholes ranged in depth from 7 meters for UTD-Coso #4 to 96 meters for UTD-Coso #6 (see Table 1).

Initial plans to leave the boreholes uncased were altered. In order to provide for long term hole stability, that is, eliminate collapse of the boreholes, and to provide more stable temperature measurements, it was deemed necessary to put "casing" in each of the boreholes (Fig. 6). A 5.1 cm diameter PVC pipe was placed in eight of the heat flow holes. In the ninth borehole, UTD-Coso #4, due to the continued collapse of the hole during drilling and the extremely shallow depth, a 7 meter section of metal casing was emplaced in the hole. UTD-Coso #2 was terminated at a depth of 23 meters and a 5.1 cm diameter steel pipe was lowered into the hole because of the high temperatures (over 40°C) measured in the drilling mud.

TABLE 1. COSO GEOTHERMAL HEAT FLOW BOREHOLE DESCRIPTIONS

Borehole Number	Location	Elevation (±10 meters)	Rock Type	Borehole Depth (meters)
UTD-Coso #1	SW 1/4 Sec 16 T22S R39E	1134	Diorite	46
UTD-Coso #2	NE 1/4 Sec 6 T21S R39E	1317	Volcanics-Alluvium	23
UTD-Coso #3	NW 1/4 Sec 19 T21S R39E	1512	Granite	18
UTD-Coso #4	NE 1/4 Sec 10 T22S R39E	1085	Alluvium	7
UTD-Coso #5	NW 1/4 Sec 2 T22S R38E	1305	Granodiorite	61
UTD-Coso #6	NW 1/4 Sec 20 T22S R39E	1268	Diorite	96
UTD-Coso #7	NW 1/4 Sec 23 T22S R38E	1097	Granite	46
UTD-Coso #8	NW 1/4 Sec 34 T21S R38E	1170	Gneiss	36
UTD-Coso #9	NW 1/4 Sec 32 T21S R38E	1542	Granite	18
UTD-Coso #10	SW 1/4 Sec 2 T22S R39E	1170	Basalt	35

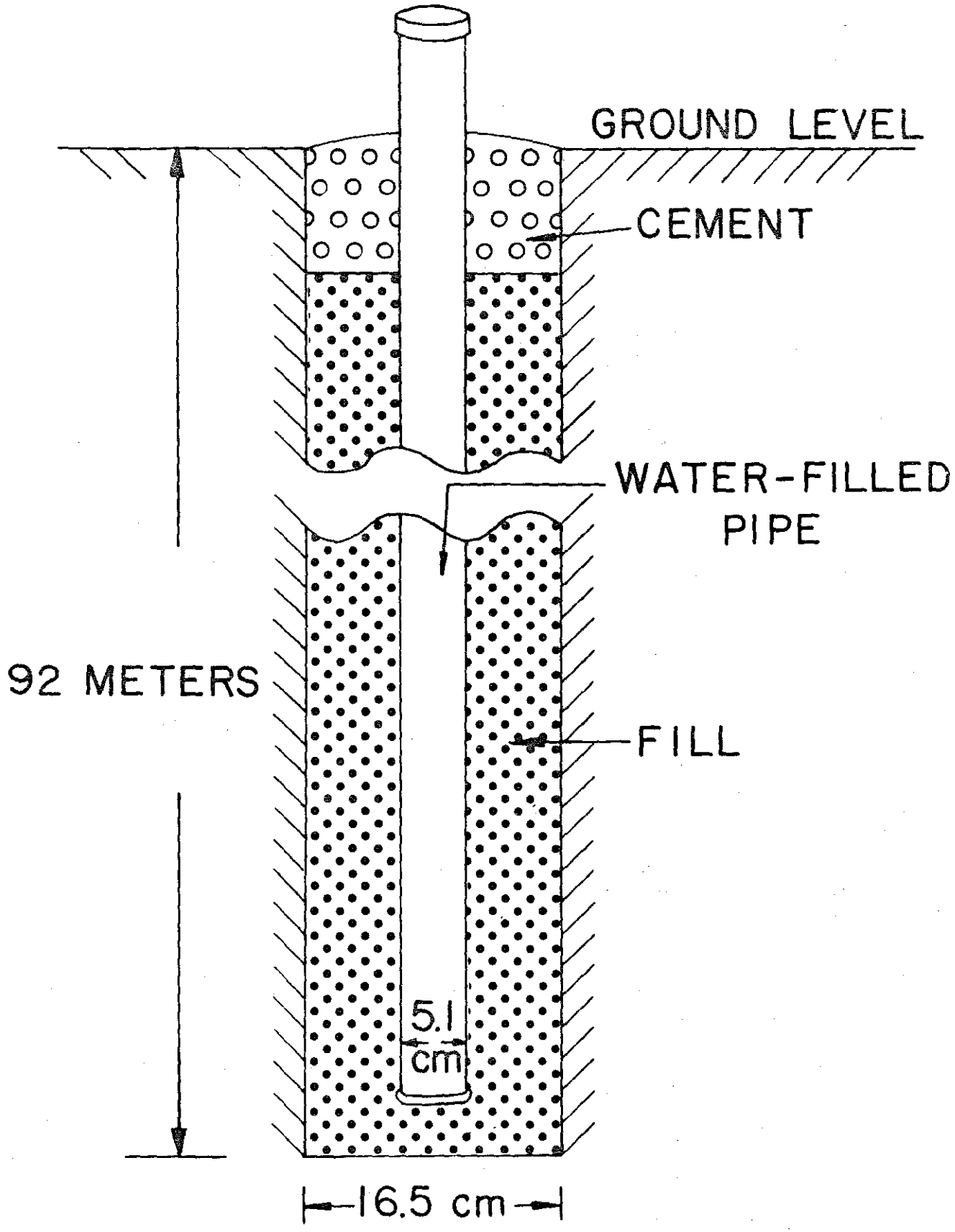

Figure 6. Schematic of heat flow borehole.

After the drilling and coring were completed, PVC pipe with a closure on both ends was lowered into the holes. Drill cuttings were caved around the pipe (See Fig. 6). The pipe was then filled with water in order to provide for thermal stability during temperature measurements by eliminating convection in the pipe.

To obtain heat flow measurements on each of these boreholes, a temperature profile was needed. In other words, measurements of temperatures as a function of depth had to be obtained. To establish the fact that the boreholes have attained equilibrium conditions, it was necessary to make at least two re-measurements in each hole. By monitoring the change of temperature as a function of time at each depth in the boreholes, equilibrium temperature gradients were determined. Temperatures were measured at discrete intervals, every 10 m, with thermistors in combination with a Wheatstone-type bridge and an electronic null detector. The bridge circuit was used with a portable, manually operated reel capable of holding 1 km of 5 mm diameter cable (Fig. 7). The temperatures were measured to within 0.01°C. Depth measurements in this study were accurate to at least 0.1%. If errors in the depth and temperature measurements are random, they cause a maximum error of 0.5% in a geothermal gradient of 150°C/km obtained over a 100 m interval.

Thermal conductivity is usually measured by one of several laboratory techniques. The most accurate technique, the divided-bar technique (Birch, 1950), requires core samples which can be machined into discs with faces smooth, flat, and parallel to 0.0025 cm (Combs and Simmons, 1973). Since only a few short cores were obtained in the present studies due to drilling costs, we have collected grab samples of the drill chips for every 3 m interval that was perforated.

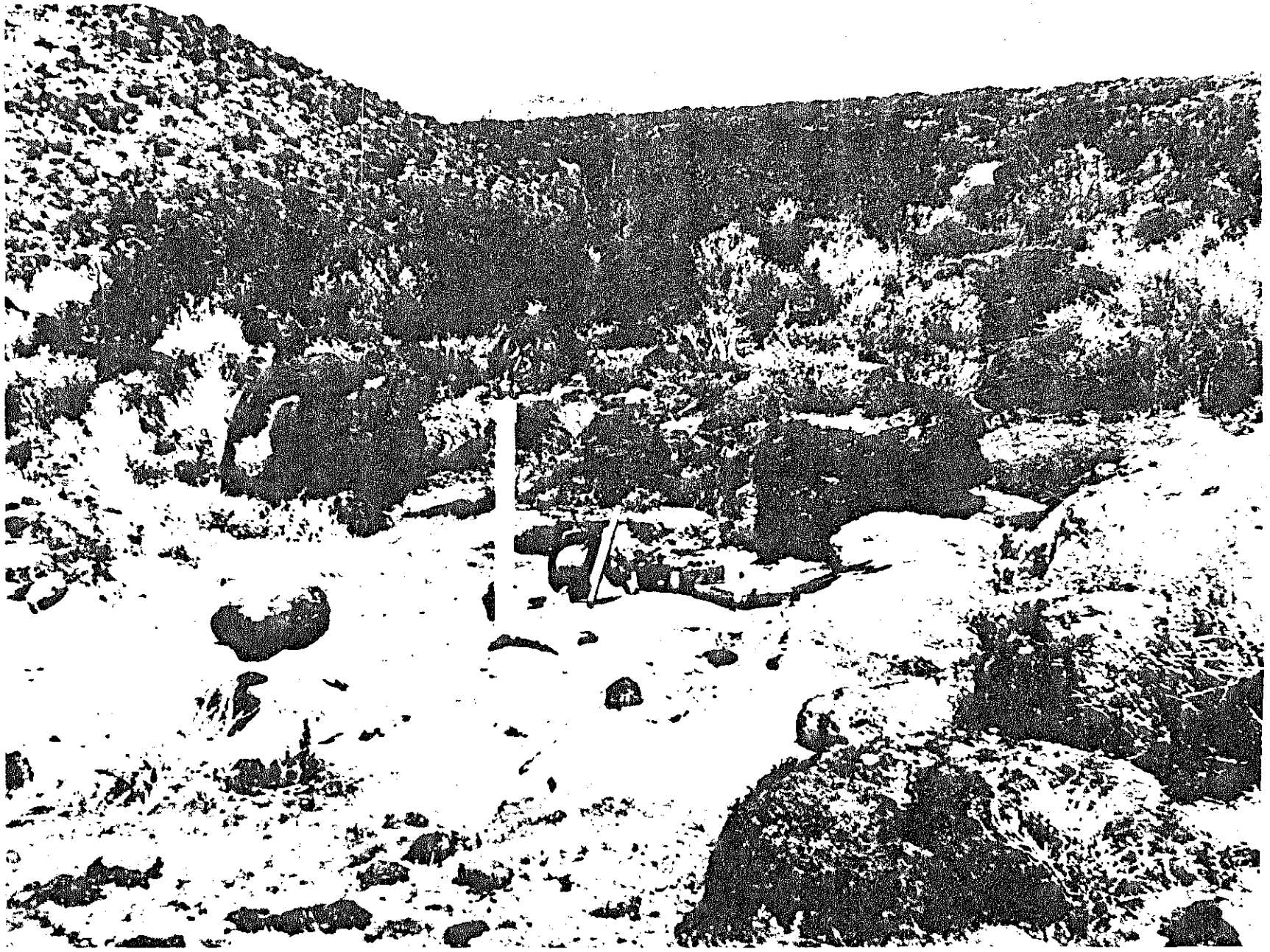

Figure 7. Heat flow borehole UTD-Coso #10. Reel, cable, and temperature measuring bridge on ground next to PVC pipe.

Both a steady state - a divided bar apparatus with a cell arrangement (Sass, et al., 1971), and a transient method - a needle probe apparatus (von Herzen and Maxwell, 1959), have been used in this investigation to determine thermal conductivities.

Thermal conductivities were measured on drill cuttings from six of the boreholes. The combined systematic and random errors in the measurement of a single grab sample are <5%, much less than the variation from specimen to specimen in most rocks. The conductivity values as functions of depth interval are tabulated in Appendix III.

HEAT FLOW RESULTS AND INTERPRETATION

Heat flow determinations are the most effective geophysical technique for locating subsurface geothermal anomalies. Broad regions of anomalously high heat flux can be defined by a few carefully located heat flow boreholes. If the regional heat flow so determined is significantly higher than normal, we can infer the presence of hydrothermal convective systems and/or young, hot intrusive rocks.

Ten sites were chosen for heat flow holes to be drilled. These locations were based on data from a detailed geothermal noise survey conducted by Teledyne Geotech (1972) and some electrical resistivity studies being conducted by Furgerson (1973). The heat flow sites were chosen such that they coincide with a number of different phenomena and combinations of phenomena from the seismic noise survey and the electrical resistivity studies. Four areas were chosen on a basis of the coincidence of the following information:

(a) high seismic noise--low electrical resistivity,

(b) high seismic noise--high electrical resistivity,

(c) low seismic noise--low electrical resistivity,

(d) low seismic noise--high electrical resistivity.

In addition to these four holes, six others were placed throughout the area in the presumed hot areas as well as in potentially non-productive areas in order to determine the magnitude of the background heat flow for the area. For example, one hole, site #10, was drilled into the basalt flows on the eastern edge of the Coso Hot Springs area. The sites (Fig. 9 and Table 1) for the ten heat flow boreholes were selected not only on the basis of the former electrical resistivity and seismic noise surveys but also in order to provide for a minimum

impact on the environment. Therefore, the ten holes were located as close as possible to existing roads with the additional constraint that they were located in bedrock. Borehole descriptions are presented in Table 1.

Temperature measurements were completed in nine of the heat flow boreholes. The tenth hole, UTD-Coso #4, was only 7 m deep and therefore no temperature measurements were made. Temperatures were measured at 5 m intervals from the ground surface to the deepest 5 m interval. Subsequently, temperatures were remeasured two or three times in each borehole in order to demonstrate that equilibrium thermal conditions existed. The maximum difference in temperature, at any of the 5 m intervals, was 0.03°C. Temperature-depth curves for seven of the boreholes are presented in Figure 8. Temperature-depth curves were not plotted for three of the boreholes, UTD-Coso #3, #4, and #9, since none of these holes penetrated deeper than 15 m. Results from these boreholes, as well as from the other seven, indicate that the temperature data above 15 m is useless for calculating the geothermal gradient. This is due to the effects of solar radiation at the surface of the earth. Separate temperature-depth curves for each of the holes are presented in Appendix I. Temperatures, as a function of depth at 5 m intervals for each borehole, are tabulated in Appendix II.

One of the questions that must be answered in the discussion of temperature gradient and heat flow determinations is what are the causes of variation. That is, what factors affect a particular heat flow value? The most important factors in the Coso Geothermal Area seem to be (1) near surface effects, (2) thermal equilibrium, and (3) groundwater movement, both hot and cold. Near surface effects, such as topography and diurnal and seasonal temperature variations caused by the heat exchange between the ground and the atmosphere, have been avoided by using only the temperature measurements taken from below 15 m in a borehole.

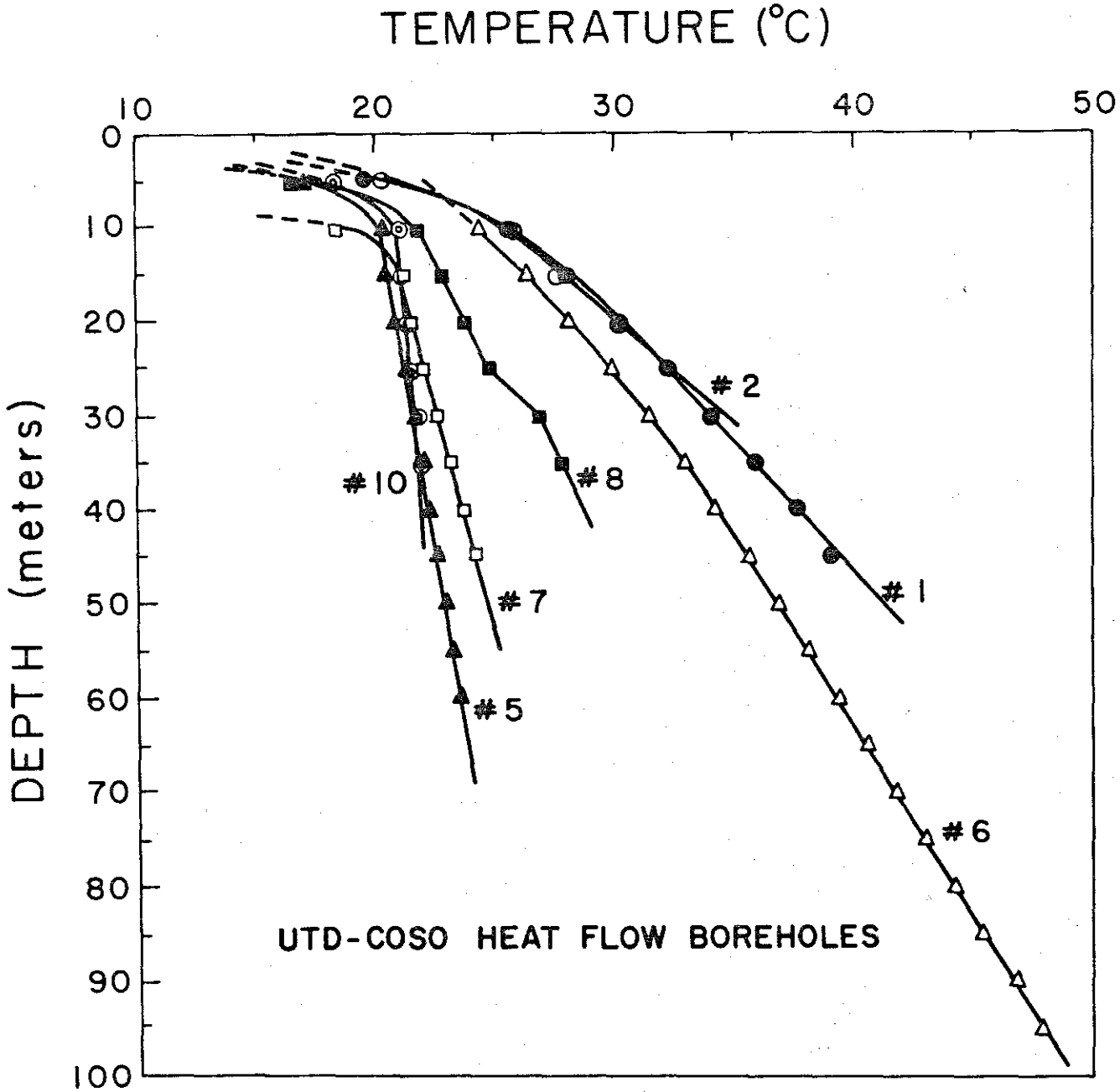

Figure 8. Temperature-depth curves for the UTD-Coso heat flow boreholes.

Adequate time was allowed for reaching thermal equilibrium in the holes disturbed by heating or cooling developed during drilling. Bullard (1947) and Jaeger (1956, 1961) have determined that the time necessary for the disturbance in temperature due to drilling to decay to 1% of its original value is 10 to 20 times the total time spent in drilling.

As can be seen from the tables and graphs, the boreholes are quite shallow (<100m). However, with extrapolation of the shallow gradients to ground level, an interface temperature of approximately 20°C is predicted, in good agreement with the mean annual surface temperature for the area of approximately 19°C. Because of the high geothermal gradients, surface thermal effects are rapidly overcome. The exception is UTD-Coso #10 with a gradient of 84.0°C/km and a temperature reversal between 5 and 15 m caused by surface thermal effects. The temperature measurements in each of the boreholes are undisturbed and indicate conductive heat transfer in the shallow subsurface. The results of the geothermal gradient, thermal conductivity, and heat flow determinations for the borehole, UTD-Coso #6, are presented in Table 2. These data indicate a constant thermal conductivity of 5.3± 0.4 mcal/cm-sec-°C for the entire 96 m depth, which is a reasonable value for diorite. Note in both Figure 8 and Table 2, the surface thermal effects extend to a depth of approximately 40 m in this borehole. Below a depth of 40 m, the geothermal gradient, thermal conductivity, and therefore the heat flow values for each 10 m interval, are quite consistent. This is indicative of a steady state thermal condition in the subsurface. Heat, in the upper 100 m of the subsurface, is being transferred by a conductive heat transfer mechanism with an absolute value of 13 $\mu cal/cm^2$-sec (13 HFU). This heat flow value is typical of geothermal systems throughout the world (Boldizar, 1963; Dawson and Fisher, 1964; Rex, 1966; Helgeson, 1968; Horai and Uyeda, 1969;

TABLE 2. HEAT FLOW DATA FOR UTD-COSO #6 HEAT FLOW BOREHOLE

DEPTH INTERVAL (m)	GEOTHERMAL GRADIENT (°C/km)	THERMAL CONDUCTIVITY (mcal/cm-sec-°C)	NUMBER OF SAMPLES	HEAT FLOW ($mcal/cm^2$-sec)
0-10	1107.0	5.2	3	58.
10-20	367.0	5.2	3	19.1
20-30	341.0	5.3	2	18.1
30-40	281.0	5.6	3	15.7
40-50	266.0	5.1	4	13.6
50-60	248.0	5.4	3	13.4
60-70	251.0	5.5	4	13.8
70-80	245.0	4.9	3	12.0
80-90	254.0	5.4	5	13.7
90-100	242.0	5.4	2	13.0

Combs, 1971) and is approximately ten times the normal terrestrial heat flow of 1.5 HFU (Lee and Uyeda, 1965; Horai and Simmons, 1969).

Appropriate depth intervals, geothermal gradients, estimated and measured thermal conductivities, and heat flow values for all holes, including the summary values for UTD-Coso #6, are shown in Table 3. Borehole locations and heat flow values are presented in Figure 9. All of these heat flow values are greater than the world average of 1.5 HFU. It should be noted that all the localities on land where heat flow has been reported in excess of 5 HFU have been obtained either on active volcanoes or in geothermal areas. For example, Boldizsar (1963) reported that the heat flow in the Larderello, Italy geothermal area varies from 6 to 14 HFU. Horai and Uyeda (1969) indicate that the conductive heat flow is 15 HFU at the Matsukawa, Japan, geothermal area; whereas, Dawson and Fisher (1964) find the heat flow as high at 40 HFU in the Wairakei, New Zealand geothermal area. Therefore, the heat flow values obtained at the Coso Geothermal Area are typical of values obtained in other geothermal areas. The Coso heat flow values are significantly higher than the worldwide average and indicate that most of the region is characterized by abnormally high subsurface temperatures and high geothermal gradients.

TABLE 3. COSO GEOTHERMAL AREA HEAT FLOW DATA

BOREHOLE NUMBER	ELEVATION (± 10 m)	DEPTH RANGE (m)	GEOTHERMAL GRADIENT (°C/km)	THERMAL CONDUCTIVITY (mcal/cm-sec-°C)	NUMBER SAMPLES	HEAT FLOW ($\mu cal/cm^2$-sec)
UTD-Coso #1	1134	20-40	359.2	5.0	10	18.
UTD-Coso #2	1317	10-20	453.8	(3.5)	-	16.
UTD-Coso #3	1512	-	No data	-	-	-
UTD-Coso #4	1085	-	No data	-	-	-
UTD-Coso #5	1305	20-60	65.9	5.1	12	3.4
UTD-Coso #6	1268	40-95	249.3	5.3	32	13.
UTD-Coso #7	1097	20-45	101.9	6.2	8	6.3
UTD-Coso #8	1170	10-25	194.0	6.4	6	12.
UTD-Coso #9	1542	-	No data	-	-	-
UTD-Coso #10	1170	15-35	84.0	4.4	9	3.7

* Number in parentheses is assumed thermal conductivity.

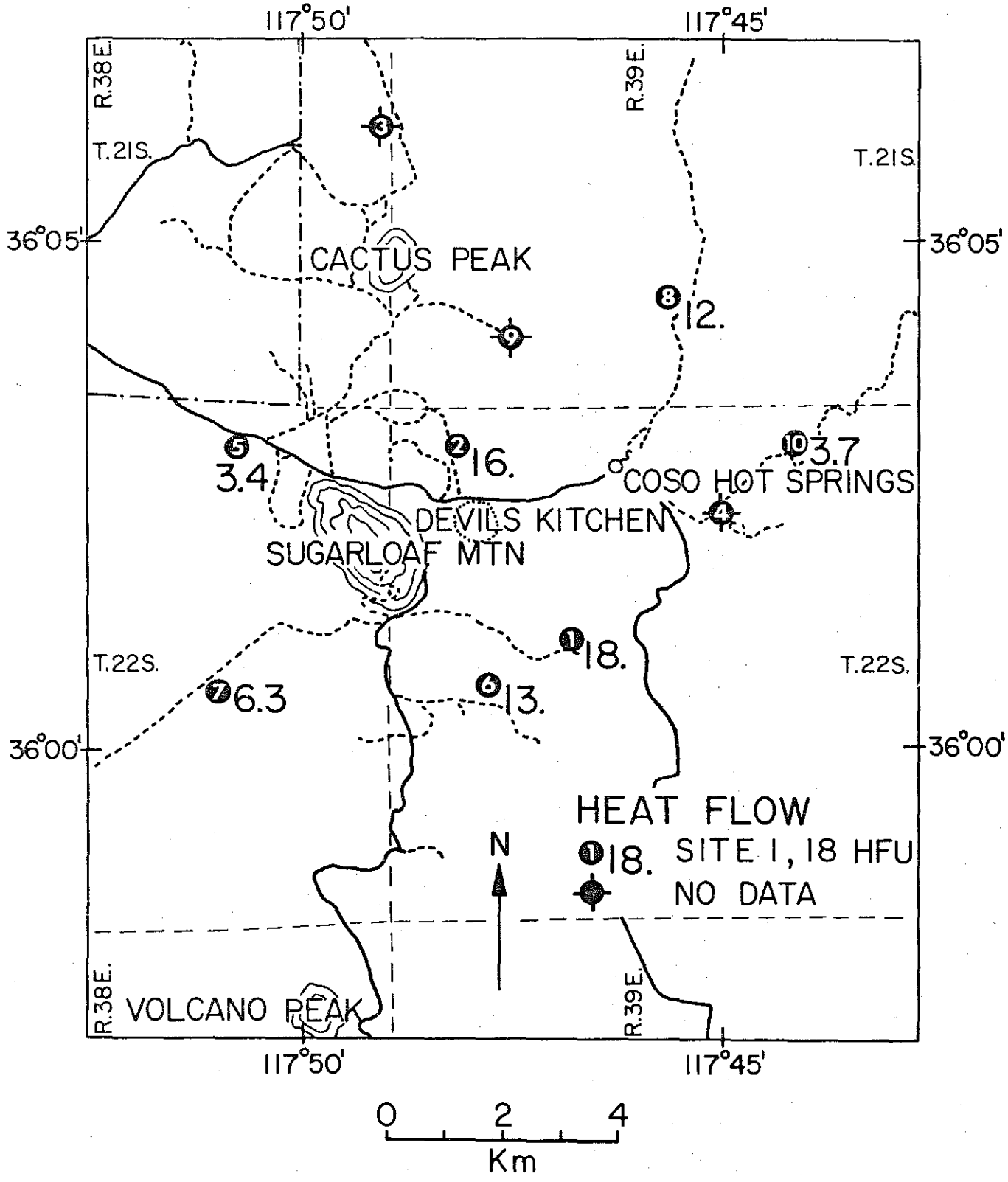

Figure 9. Borehole locations with heat flow determinations in units of $\mu cal/cm^2$-sec. The symbol ✦ indicates that no geothermal gradient was obtainable from the borehole.

MICROEARTHQUAKE INSTRUMENTATION AND FIELD PROCEDURE

An array of six Kinemetrics PS-1 portable vertical-component high-gain seismographs (Prothero and Brune, 1971) was established in the Coso Geothermal Area. Several internal filters provided with the seismographs, can be used to shape the system response. Filter 1, peaked at 1 Hz, produced easily discernible first motions, although it probably reduced the number of small local microearthquakes that were recorded since the high frequency waves from these events are mostly filtered out. Higher resolution of events, and well-defined S-P interval times, were obtained by using filter 4 peaked at 20 Hz, which is the predominant frequency for very near microearthquakes. Gain was controlled by attenuating the maximum system sensitivity in 6-db steps. Stations operated on filter 4 were attenuated from 24 to 36 db, whereas the same stations could be operated on filter 1 with about 12 db less attenuation. Recording was accomplished at 1 mm/sec with smoked paper drum recorders.

Kinemetrics Ranger seismometers with a natural frequency of 1 Hz were used. The average generator constant for these seismometers was 100 V-sec/m. External resistors damped the system at 0.7 critical. Timing for the recording units was provided by a temperature-compensated, crystal-controlled unit with an accuracy of ±0.3 ppm over the temperature range of 0°C to 50°C. Timing was reestablished daily at each station by superimposing the National Bureau of Standards WWV time code with the internal clock on each record. The drum speed and accurate timing permitted P arrivals to be picked to 0.1 sec. Without horizontal instruments, S phases could not be clearly distinguished from multiple crustal P phases and therefore were not used in hypocentral locations.

Five of these smoked paper drum recorders were installed on June 13 and 14 while a sixth was installed on June 20, 1974. All of these recorders were picked up on the 25th of June, 1974. Out of the twelve days of recording, ten included information which was sufficient to determine the initial character of the micro-earthquake activity in the area.

During the period July 5 to July 27, 1974, nine, custom made, three-component, high-gain, magnetic tape recorder type seismographs were installed in the area. Six of these instruments were placed at the locations occupied by the original smoked paper seismographs. Each package consisted of three Texas Instruments seismometers to measure the vertical and two orthogonal horizontal components of ground motion, and a magnetic tape recording unit. The seismometers were critically damped and resonant frequencies were 2 Hz for the vertical instrument and 2.5 Hz for the horizontal instruments. Each seismometer was equipped with a preamplifier with a flat gain response of 400 between the 0.5 Hz to 40 Hz pass band. Input noise was less than 0.5 μV in the pass band of 2 to 20 Hz. The recording units were built at The University of Texas at Dallas. Each unit recorded six channels (Fig. 10) in analog format on standard 8.9 cm or 12.7 cm reels of magnetic tape via a Norton Industries tape head. The outer two channels record coded time signals from an internal digital clock. This is done to insure that a timing signal is recorded, and to correct for timing errors due to tape skewness. The internal clocks were accurate to about 0.1 ppm, or one second per month. One of the four inner channels was used to record a time segment from radio WWV and a portable traveling clock at the beginning and end of each tape. This established an absolute time base and allowed for correction of internal clock drift. The remaining three channels were used for recording the seismic signals from the three seismometers.

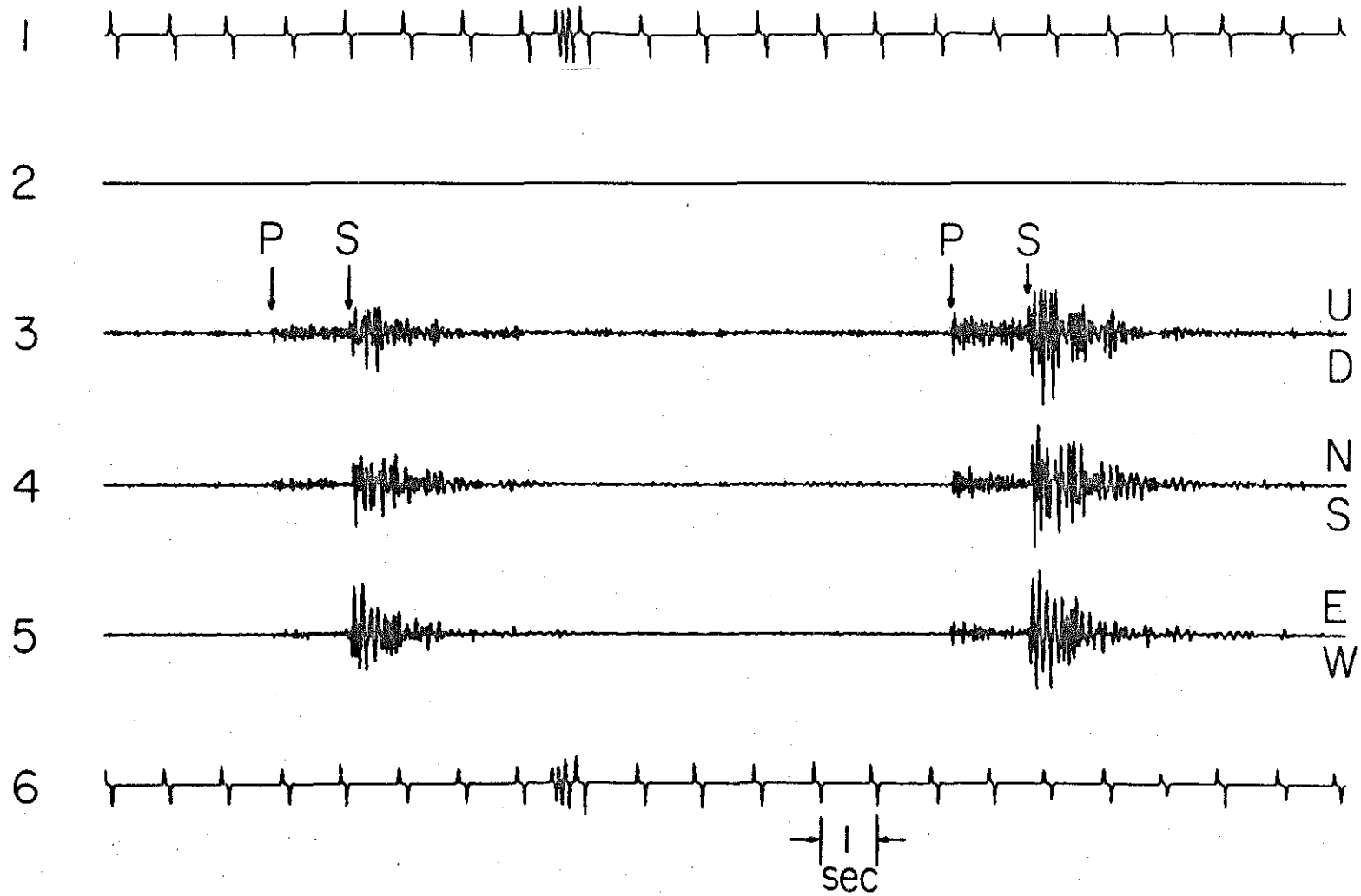

MICROEARTHQUAKE SEISMOGRAM, COSO GEOTHERMAL AREA

SEISMOGRAPH STATION # 7 JULY 7, 1973

Figure 10. Microearthquake seismogram for station #7, Coso Geothermal Area. Channels 1 and 6 are internal clock channels. Channel 2 is reserved for WWV and traveling clock times at the beginning and end of the magnetic tape. Channel 3 is the vertical component of ground motion, 4 and 5 are orthogonal horizontal components.

The seismic amplifiers in the recording units have a continuously variable gain from 1 to 100. Gain was set at the recording site so that the peak-to-peak ground noise was approximately 1 mV. The amplified seismic signal is mixed with an 800 Hz bias signal with amplitude set at 1.2 V.

We recorded for 23 days and obtained usable data from eight of these three-component magnetic tape units. The important differences between the two types of seismographs are (1) three component (one vertical and two horizontal) versus a single component (vertical) installation and (2) the magnetic tape recorders versus the smoked paper drum recorders. The three components provided for excellent resolution in the picking of the S-wave arrivals and consequently the S-P time intervals (Fig. 10). The magnetic tape enabled us to play back the records at different speeds to provide for more distinct P- and S-wave arrivals.

MICROEARTHQUAKE RESULTS AND INTERPRETATION

We have conducted both active and passive field work in the area. From these studies we wanted to determine the background level of seismicity associated with the Coso Geothermal Area prior to the onset of potential effects caused by future production and reinjection of fluids into presumed geothermal reservoirs. In addition, from the microearthquake activity and precise hypocentral estimates, it is possible to determine any active fault zones in the area which may be functioning as subsurface conduits. Finally, the present microearthquake survey will be used to speculate on the subsurface physical characteristics of the Coso geothermal system.

The microearthquake activity changed considerably over these periods of recording, including some days which had only a few events while others included as many as one hundred or more distinct local events per day. In order to quantify the seismicity of the Coso Geothermal Area, we counted events with S-P times of less than 3 seconds for the station near Cactus Peak (Station #2 in Fig. 14). Intermittent high noise during the local daytime made event counting less certain; therefore, we have plotted only the number of events per day for the 12-hour period between 2100 and 1900 local time (Fig. 11). Strain release in the Coso Geothermal Area seems to occur primarily in swarm-type sequences as can be noted by the continuous occurrence of microearthquakes, whereas earthquakes outside the area occur primarily as mainshock-aftershock sequences. The area is definitely undergoing current tectonism.

During laboratory studies of microfracturing, Mogi (1963) and Scholz (1968) noted that stress inhomogeneities, related to either inhomogeneous materials or concentrated sources, are correlated with high b values and with swarm-like sequences. Thus, earthquake swarms associated with geothermal areas may be indicative of magmatic activity in progress. That is, swarms may reflect either

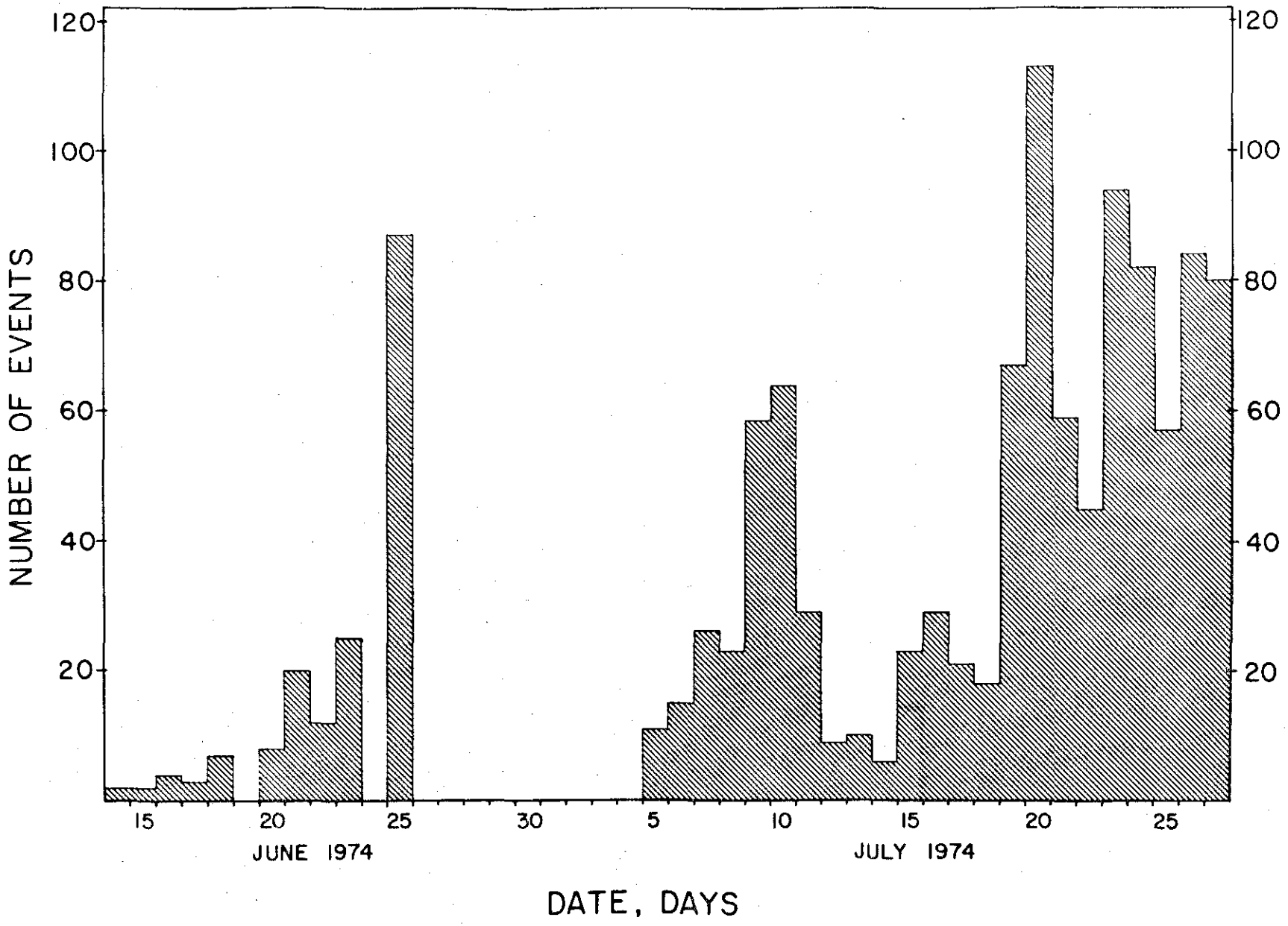

Figure 11. Seismicity of the Coso Geothermal Area. Number of events with S-P times of less than 3 seconds for station #2 near Cactus Peak for the 12-hour period between 2100 and 0900 local time.

magmatic activity that does not reach the surface of the earth as volcanic eruptions, or hydrothermal processes that trigger tectonic strain release.

Rinehart (1972) has suggested that deformational strain generated by earth tidal forces in geyser basins could be expected to influence heat flow variation resulting in crack and fissure dilatation allowing convective geothermal fluids to permeate the surrounding material. This mechanism could account for the formation of steam and increased water temperature in the subsurface that would in turn decrease the effective stress enough to allow fracture and produce small earthquakes.

To provide a more realistic subsurface velocity model and to aid in the determination of the accuracy of the microearthquake hypocenters, calibration shots provided by personnel of the Naval Weapons Center were analyzed. The shots were located within 250 m. The resulting time-distance plot (Fig. 12) indicates an essentially constant P-wave velocity of 4.75 km/sec which is in excellent agreement with the seismic refraction studies of Zbur (1963) in the Indian Wells Valley immediately to the south. From a combination of our data, the refraction data of Zbur (1963), and the crustal model of Prodhel (unpublished data) derived from a reversed refraction profile from China Lake to Mono Lake, we obtained a crustal model which consists of a 5.0 km thick layer with a velocity of 4.75 km/sec overlying a half space of 6.0 km/sec. On many of the seismograms, the S-arrival is impulsive and clear while the P-arrival is emergent. The background noise is more pronounced in the spectral band of P-waves compared to that for S-waves. Therefore, it is advantageous to be able to use the S-phase with some confidence as to its velocity of propagation. The S-velocity can be obtained from the P-velocity through the well known Wadati diagram (Kisslinger and Engdahl, 1973).

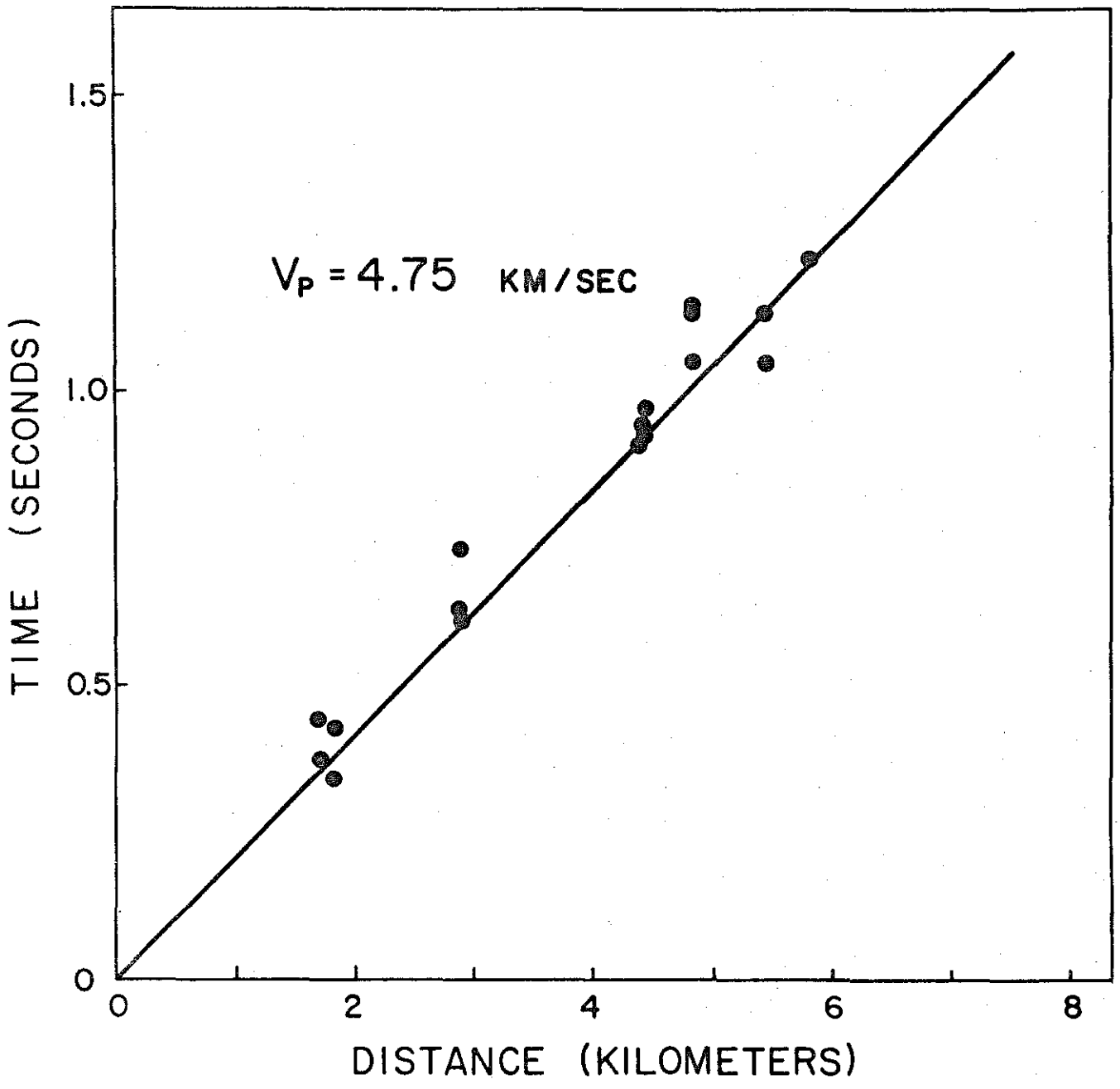

Figure 12. Time-distance curve for calibration blasts.

Wadati diagrams, S-P times plotted against P-arrival times, were originally drawn to find Poisson's ratio for rocks under stress. The graph was then extrapolated to an S-P time of zero which yields the earthquake origin time.

In equation form, we have for the Wadati diagram,

$$S\text{-}P = (P\text{-}0)\ (K\text{-}1) \qquad \ldots\ldots\ldots\ldots\ldots\ldots\ (1)$$

where

S = S-wave arrival time

P = P-wave arrival time

0 = Origin time

and

$$K = V_P/V_S$$

where

V_P = P-wave velocity

V_S = S-wave velocity

Note that S-P time plotted against P-wave arrival time yields a straight line with a slope K-1. Normally, in the construction of a Wadati diagram, the data from one event recorded at many stations is used. By expanding equation (1), we obtain an equation of the form

$$S = PK - 0\ (K\text{-}1) \qquad \ldots\ldots\ldots\ldots\ldots\ldots\ (2)$$

In this form, where S-arrival time is plotted against P-wave arrival, if we drop the second term, we get the reduced Wadati diagram. For the reduced Wadati diagram, all of the values of S-arrival time and P-arrival time for several events are reduced to one station. We have plotted reduced S-arrival time, S_R, versus reduced P-arrival time, P_R, for a number of events (Fig. 13). From a least squares linear regression analysis, we obtain a slope of 1.57. The ratio

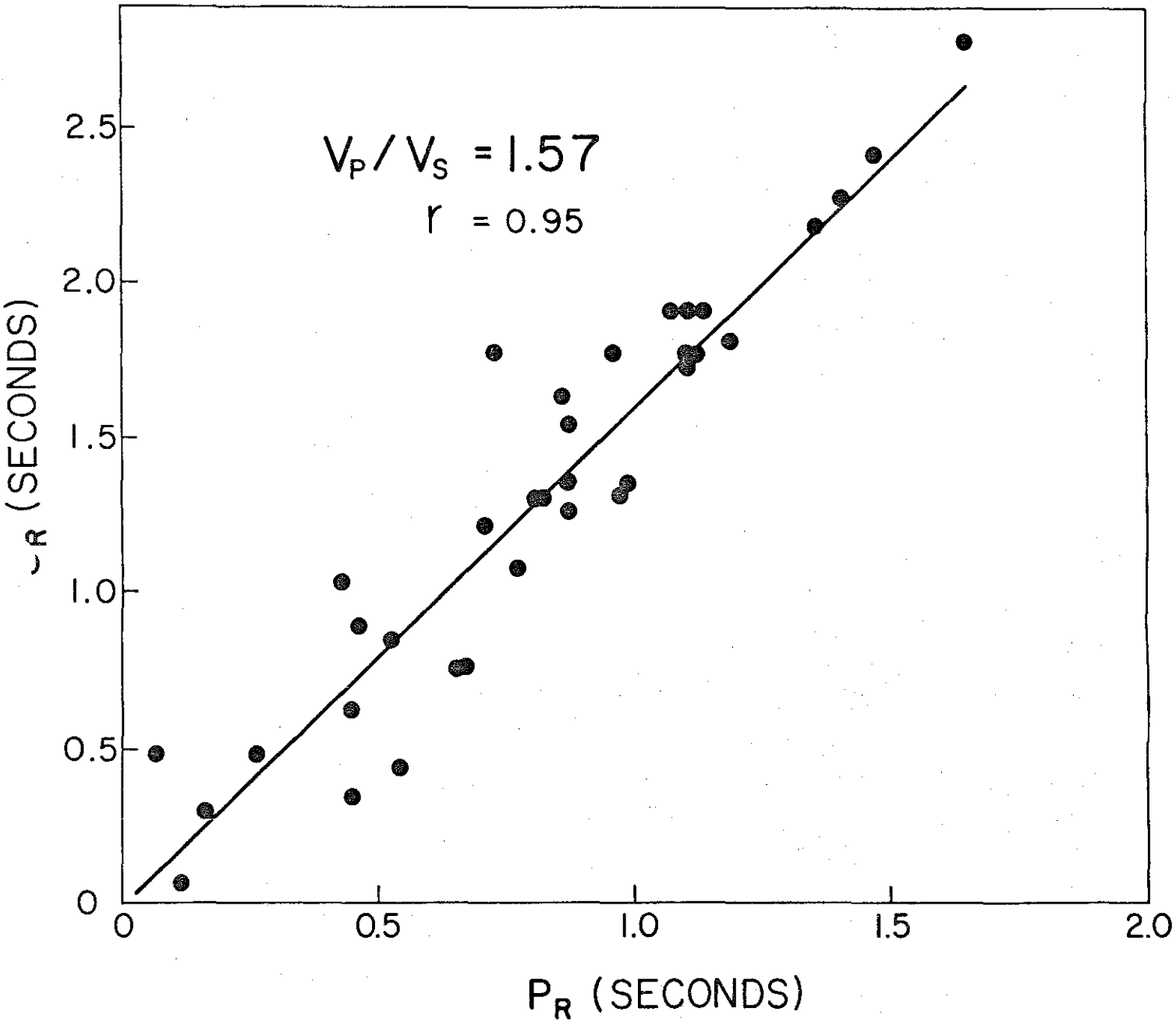

Figure 13. Reduced Wadati diagram. All values of S-arrival time and P-arrival time for several events are reduced to one station and plotted as reduced S-arrival time, S_R, versus reduced P-arrival time, P_R.

of V_P to V_S is therefore equal to 1.57 compared to values of 1.73 to 1.87 which are usually obtained in laboratory and field investigations. Using the P-wave velocity of 4.75 km/sec determined from the calibration blasts, we obtained an S-wave velocity of 3.30 km/sec. These velocities infer a Poisson's ratio of 0.16 compared with values 0.25 to 0.30 which are normally observed.

In a series of carefully performed laboratory experiments, Nur and Simmons (1969) have observed the effect of saturation on seismic velocity in low porosity rocks. They found that fluid saturation greatly influences the effective bulk modulus of rocks while the shear modulus is almost independent of fluid inclusions. In other words, the shear wave velocity is almost unchanged when the air in cracks is replaced by water whereas the compressional wave velocity may increase by as much as 40% for rocks with porosities of less than 0.01. Furthermore, Nur and Simmons (1969) noted that dry rocks exhibit very low values of Poisson's ratio (<0.20) while saturated rocks exhibit normal to high values ($\geq$0.25).

The low value for Poisson's ratio observed for the Coso Geothermal Area indicates that the shallow subsurface is either deficient in liquid water saturation or more likely that the void spaces (cracks) are filled with steam. These results imply that the Coso geothermal system is a vapor-dominated system rather than a hot-water system.

Using all of the above mentioned data in a program written by Lee and Lahr (1972), we have located 78 microearthquakes ranging in magnitude from -1.0 to 2.5 out of the hundreds which were recorded (Fig. 14). These 78 microearthquakes include events obtained on both seismograph systems as well as events occurring throughout the total recording interval. Most of the seismic

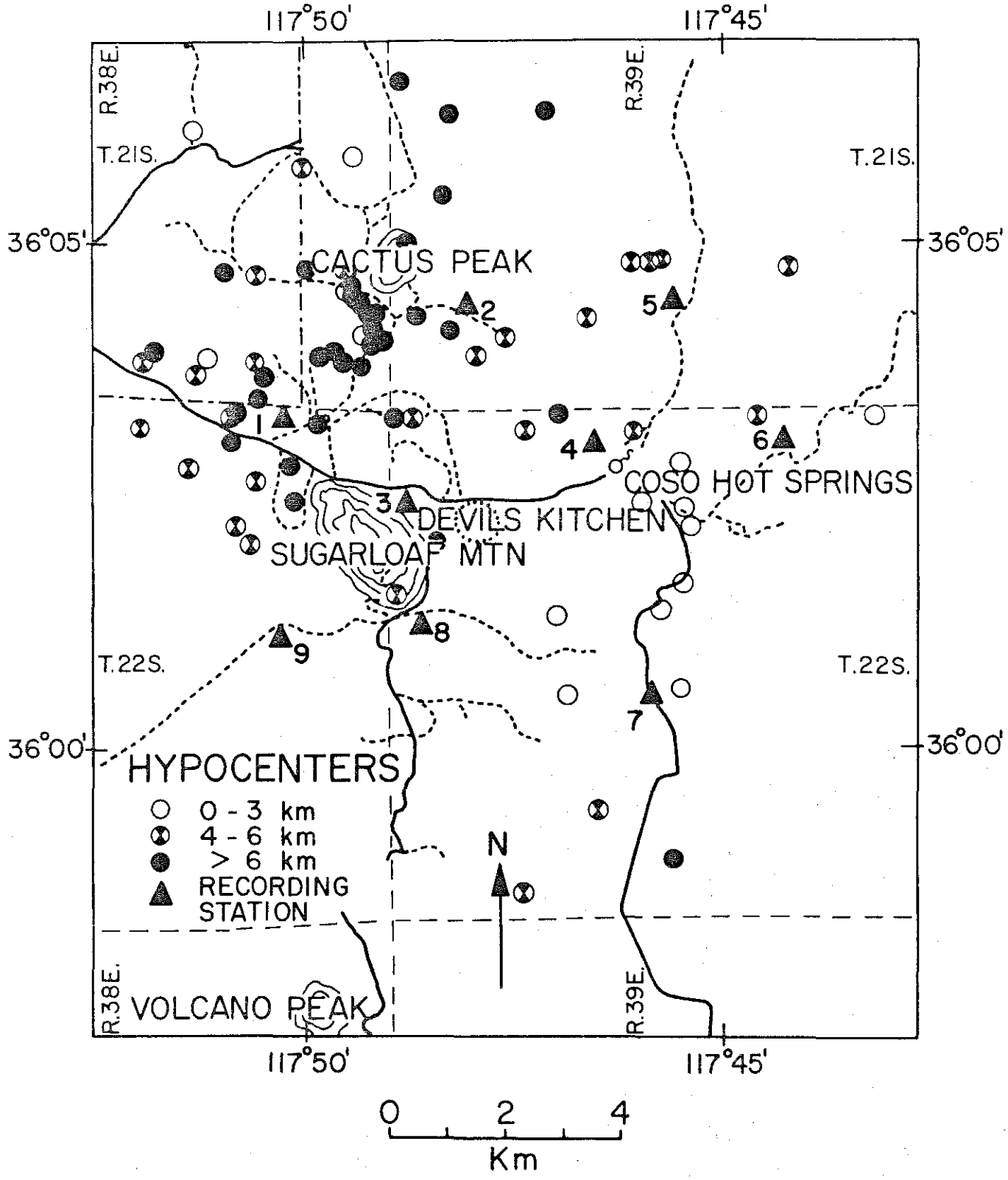

Figure 14. Epicenters of 78 microearthquakes associated with the Coso Geothermal Area.

activity occurred between the two young volcanoes, Cactus Peak (97,000 yrs; Lanphere, et al., 1975) and Sugarloaf Mountain (40,000 yrs; Lanphere, et al., 1975), although all surface manifestations are observed around Coso Hot Springs and to the east of Devil's Kitchen. Note the position of the epicenters with respect to the thermal manifestations. Events clustered around the Coso Hot Springs and extending to the south are all shallow with focal depths between 1 and 3 km. Focal depths increase from the Coso Hot Springs area toward the west and northwest. Most of the events were located in the western portion of the Coso Geothermal Area near the zone of volcanic manifestations, that is, near the perlite domes. These events are usually deeper ranging from 5 to 10 km. There appears to be a positive correlation between areas of high seismic noise (Fig. 3) and areas of microearthquake activity (Fig.14) as well as an inverse correlation between the focal depth and the amplitude of the noise.

We have obtained a fault plane solution for the shallow events in the Coso Hot Springs area and those to the south (Fig. 14) The resulting focal mechanism clearly indicates a right-lateral strike-slip fault which has a north-south strike (Fig. 15). Although a unique choice of the fault plane cannot be made from the first motion data, the north striking plane was chosen due to the alignment of the epicenters.

Finally, microearthquakes clustering around the Cactus Peak area (Fig. 14) were examined in an effort to compare the relative attenuation of events arriving at the seismograph sites along different ray paths (Walsh, 1969). Ray paths, between Cactus Peak and seismograph sites #3, #8, and #7 pass through an anomalously high temperature, shallow crustal zone, whereas they do not from Cactus Peak to station #5 (Fig. 9).

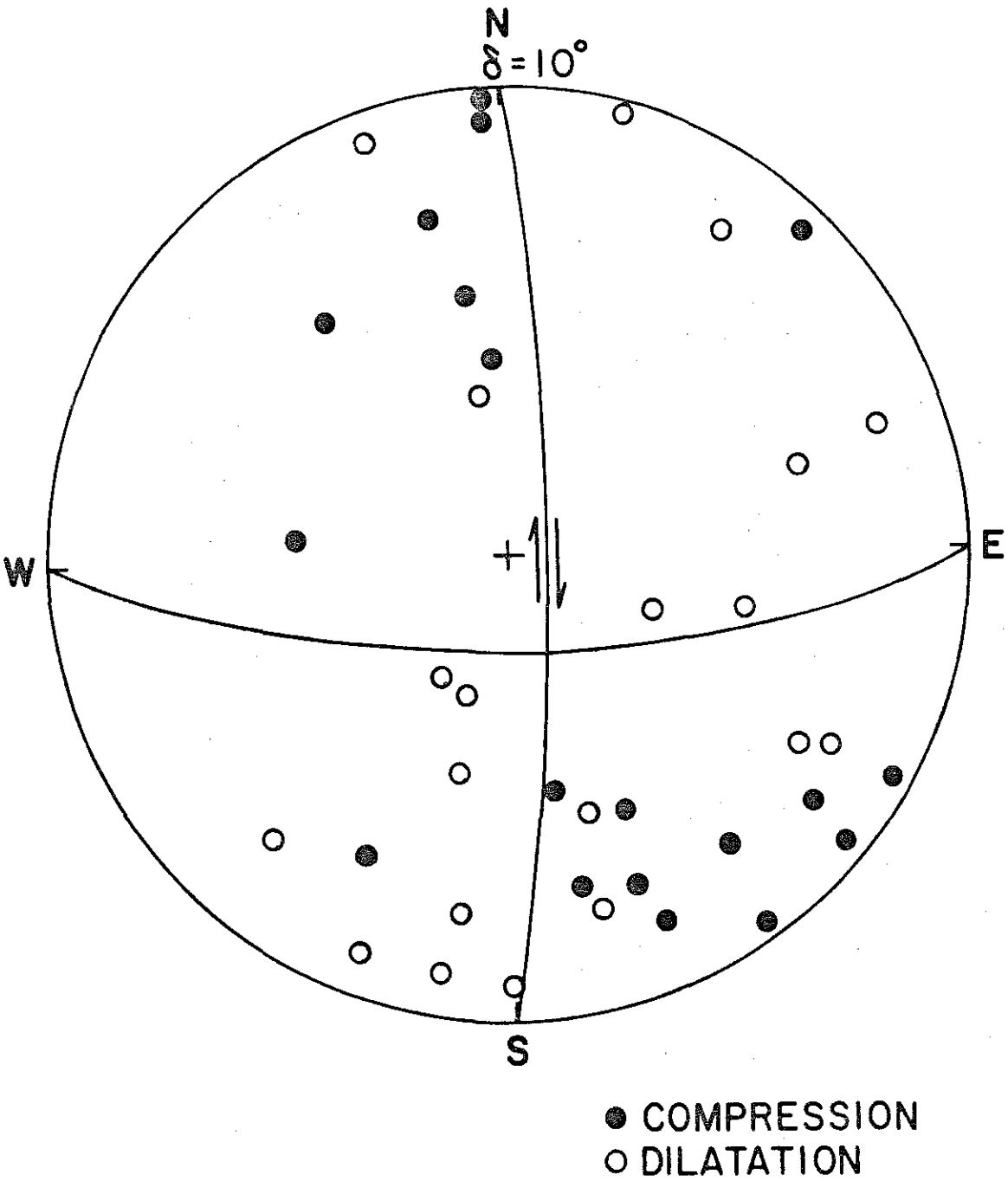

Figure 15. Lower hemisphere equal-area plot of data for fault plane solution of shallow events near Coso Hot Springs.

Since P- and S-residuals from well located microearthquakes usually range from -0.02 to 0.02 seconds, anomalous ones are easy to pick. At seismograph station #7, the P-arrivals for eight events studied arrived slightly early, while the S-phase was quite late. Station #7 is at least 10 km from the hypocentral region for the Cactus Peak events. Ray paths may pass through regions with quite different ratios of V_P to V_S which would explain the P- and S-residuals.

The S-phases are attenuated at stations #3, #8, and #7 indicating that the elastic waves have passed through a high temperature, shallow crustal zone (Solomon, 1973). Similar phenomena are not apparent on records obtained at seismograph site #5. All of these characteristics indicate a local geologic body with properties different from those of its surroundings. These anomalous seismic phenomena substantiate the high heat flow data obtained (Fig. 9).

CONCLUSIONS

The Coso Geothermal Area consists of a domed granitic basement with both young calcic and silicic volcanic eruptions situated on the granitic rocks. Heat is indicated by a combination of hot springs, fumaroles, high heat flow, high temperatures at shallow depths, low electrical resistivity values, anomalous subsurface elastic properties obtained from microearthquake studies, and a broad regional structural fabric suggesting a caldera-like feature with an underlying magma chamber.

Comparisons with the surface geophysical data obtained from presently exploited geothermal reservoirs, e.g., Larderello and The Geysers, indicate that the Coso Geothermal Area has a unique mixture of favorable features viewed individually and in combination. The Coso geothermal system appears to have the potential for production of hot brines from shallow zones, for production of dry steam, and for areas of hot dry rock. Whatever new data is provided by future surface geothermal investigations or drilling, the existence of the large, late Cenozoic ring structure centered around the active fumaroles and areas of Pleistocene volcanism defined by Duffield (1975) as well as the present heat flow and microearthquake studies provide a much larger target for geothermal exploration than suggested by the distribution of the hot springs, fumaroles, and young volcanic rocks.

Significant geological, geochemical and geophysical investigations have already been accomplished. However, a comprehensive geological, hydrological, geochemical, and geophysical evaluation of the Coso Geothermal Area should be completed to produce a well documented case history and realistic model of the Coso geothermal system.

Future geological, geochemical, and geophysical studies are planned by scientists at the United States Geological Survey, The University of Texas at Dallas, Battelle Pacific Northwest Laboratories, and the China Lake Naval Weapons Center. These include detailed geologic mapping with radiometric age dating, geochemical studies, a detailed telluric survey, AFMAG and magnetotelluric soundings, passive seismic studies including P-delays and seismic noise, completion of detailed gravity and aeromagnetics, geodetic studies, as well as additional microearthquake and heat flow investigations. Experience has demonstrated, however, that surface geophysical exploration techniques are not adequate in themselves for evaluating geothermal resources. The existing slim hole drilling technology should be used as a primary exploration tool in conjunction with geophysical surface surveys since parameters such as temperature, pressure, porosity, permeability, flow rates, etc., of presumed geothermal reservoirs can only be obtained from drill holes. In fact, during the very near future some 2 to 5 slim holes will be drilled to depths of up to 2 km in the Coso Geothermal Area in order to substantiate the information obtained from surface and near-surface geophysical surveys and to provide estimates of the geothermal reservoir characteristics.

ACKNOWLEDGMENTS

I wish to express my thanks to Carl F. Austin, Royce Coleman, Jean Davidson, R. N. Delaloye, Fumiko Goss, Ronald D. Goss, Harsh K. Gupta, Donald W. Klick, J. K. Pringle, Yair Rotstein, and Mike Wilt for their assistance, comments and criticism at various stages of the project.

REFERENCES

Austin, C. F., Austin, W. H., Jr., and Leonard, G. W., 1971, Geothermal science and technology - A national program: Naval Weapons Center Tech. Ser. 45-029-72, 95 pp.

-----, and Pringle, J. K., 1970, Geologic investigations at the Coso thermal area: Naval Weapons Center Tech. Pub. 4878, 40 pp.

Birch, F., 1950, Flow of heat in the Front Range, Colorado: Geol. Soc. Amer. Bull., v. 61, p. 567-630.

Boldizsar, T., 1963, Terrestrial heat flow in the natural steam field at Larderello: Geofs. Pura Appl., v. 56, p. 115-122.

Brune, J. N., and Allen, C. R., 1967, A micro-earthquake survey of the San Andreas Fault system in Southern California: Bull. Seism. Soc. Am., v. 57, p. 277-296.

Bullard, E. C., 1947, The time necessary for a borehole to attain temperature equilibrium: Monthly Notices Roy. Astron. Soc. Geophys. Suppl., v. 5, p. 127-130.

Combs, J., 1971, Heat flow and geothermal resources estimates for the Imperial Valley: In Cooperative geological-geophysical-geochemical investigations of geothermal resources in the Imperial Valley area of California, Univ. Calif., Riverside, Education Research Service, p. 5-27.

-----, and Simmons, G., 1973, Terrestrial heat flow determinations in the North Central United States: J. Geophys. Res., v. 78, p. 441-461.

-----, and Hadley, D., 1976, Microearthquake investigation of the Mesa Geothermal Anomaly, Imperial Valley, California: Geophysics, v. 41, in press.

Dawson, G. B., and Fisher, R. G., 1964, Diurnal and seasonal ground temperature variations at Wairakei: New Zealand J. Geol. Geophys., v. 7, p. 144-154.

Duffield, W. A., 1975, Late Cenozoic ring faulting and volcanism in the Coso Range area of California: Geology, v. 3, p. 335-338.

Evernden, J. F., Savage, D. E., Curtis, G. H., and James, G. T., 1964, Potassium-argon dates and the Cenozoic mammalian chronology of North America: Am. Jour. Sci., v. 262, p. 145-198.

Frazer, H. J., Wilson, H.B.D., and Hendry, N. W., 1943, Hot springs deposits of the Coso Mountains, California: Jour. Mines and Geol., v. 38, p. 223-242.

Furgerson, R. B., 1973, Progress report on electrical resistivity studies, Coso geothermal area, Inyo County, California: NWC TP 5497, 38 pp.

Godwin, L. H., Haigler, L. B., Rioux, R. L., White, D. E., Muffler, L. J. P., and Wayland, R. G., 1971, Classification of public lands valuable for geothermal steam and associated geothermal resources: U. S. Geol. Survey Circ. 647, 18 pp.

Hamilton, R. M., and Muffler, L.J.P., 1972, Microearthquakes at the Geysers geothermal area, California: J. Geophys. Res., v. 77, p. 2081-2086.

Helgeson, H. C., 1968, Geologic and thermodynamic characteristics of the Salton Sea geothermal system: Am. Jour. Sci., v. 266, p. 129-166.

Hileman, J. A., Allen, C. R., and Nordquist, J. M., 1973, Seismicity of the southern California region, 1 January 1932 to 31 December 1972: Seism. Lab., Cal. Inst. Tech., 492 pp.

Horai, K., and Simmons, G., 1969, Spherical harmonic analysis of terrestrial heat flow: Earth Planet. Sci. Lett., v. 6, p. 386-394.

-----, and Uyeda, S., 1969, Terrestrial heat flow in volcanic areas: in Geophysical Monograph No. 13, The Earth's Crust and Upper Mantle, ed. by P. J. Hart, Amer. Geophys. Union, Washington, D. C., p. 95-109.

Jaeger, J. C., 1956, Numerical values for the temperature in radial heat flow: J. Math. Phys., v. 34, p. 316-321.

-----, 1961, The effect of the drilling fluid on temperatures measured in boreholes: J. Geophys. Res., v. 66, p. 563-569.

Kisslinger, C., and Engdahl, E. R., 1973, The interpretation of the Wadati diagram with relaxed assumptions: Bull. Seism. Soc. Am., v. 63, p. 1723-1736.

Koenig, J. B., Gawarecki, S. J., and Austin, C. G., 1972, Remote sensing survey of the Coso geothermal area, Inyo County, California: Naval Weapons Center Tech. Pub., 5233, 32 pp.

Lange, A. L., and Westphal, W. H., 1969, Microearthquakes near the Geysers, Sonoma County, California: J. Geophys. Res., v. 74, p. 4377-4378.

Lanphere, M. A., Dalrymple, G. B., and Smith, R. L., 1975, K-Ar ages of Pleistocene rhyolitic volcanism in the Coso Mountains, California: Geology, v. 3, p. 339-341.

Lee, W. H. K., and Uyeda, S., 1965, Review of heat flow data: in Geophysical Monograph No. 8, Terrestrial heat flow, ed. by W. H. K. Lee, Amer. Geophys. Union, Washington, D. C., p. 87-190.

-----, and Lahr, J. C., 1972, HYPO71: A computer program for determining hypocenter, magnitude, and first motion pattern of local earthquakes: U. S. Geol. Surv. Open File Report, Menlo Park, 100 pp.

Mogi, K., 1963, Some discussions on aftershocks, foreshocks, and earthquake swarms - The fracture of a semi-infinite body caused by an inner stress origin and its relation to the earthquake phenomena, 3: Bull. Earthq. Res. Inst., v. 41, p. 615-658.

Nur, A., and Simmons, G., 1969, The effect of saturation on velocity in low porosity rocks: Earth Planet. Sci. Lett., v. 7, p. 183-193.

Prothero, W. A., and Brune, J. N., 1971, A suitcase seismic recording system: Bull. Seism. Soc. Am., v. 61, p. 1849-1853.

Rex, R. W., 1966, Heat flow in the Imperial Valley of California (abstr.): Am. Geophys. Union Trans., v. 47, p. 181.

Rinehart, J. S., 1972, Fluctuations in geyser activity caused by variations in earth tidal forces, barometric pressure, and tectonic stresses: J. Geophys. Res., v. 77, p. 342-350.

Sass, J. H., Lachenbruch, A. H., and Munroe, R. J., 1971, Thermal conductivity of rocks from measurements on fragments and its application to heat-flow determinations: J. Geophys. Res., v. 76, p. 3391-3401.

Scholz, C. H., 1968, The frequency-magnitude relation of microfracturing in rock and its relation to earthquakes: Bull. Seism. Soc. Am., v. 58, p. 399-415.

Solomon, S. C., 1973, Shear wave attenuation and melting beneath the Mid-Atlantic Ridge: J. Geophys. Res., v. 78, p. 6044-6059.

Teledyne Geotech, 1972, Geothermal noise survey of the Coso Hot Springs area, Naval Weapons Center, China Lake, CA: unpublished Technical Report. No. 72-6 produced under contract for the Naval Weapons Center, 18 pp.

von Herzen, R., and Maxwell, A. E., 1959, The measurement of thermal conductivity of deep-sea sediments by a needle-probe method: J. Geophys. Res., v. 64, p. 1557-1563.

Walsh, J. B., 1969, New analysis of attenuation in partially melted rock: J. Geophys. Res., v. 74, p. 4333-4337.

Ward, P. L., 1972, Microearthquakes: Prospecting tool and possible hazard in the development of geothermal resources: Geothermics, v. 1, p. 3-12.

-----, and Björnsson, S., 1971, Microearthquakes, swarms, and the geothermal areas of Iceland: J. Geophys. Res., v. 76, p. 3953-3982.

-----, and Jacob, K. H., 1971, Microearthquakes in the Ahuachapan geothermal field, El Salvador, Central America: Science, v. 173, p. 328-330.

-----, Pálmason, G., and Drake, C., 1969, Microearthquake survey and the mid-Atlantic Ridge in Iceland: J. Geophys. Res., v. 74, p. 665-684.

Westphal, W. H., and Lange, A. L., 1962, Project San Andreas Aftershock Recording, Fairview Peak Area of Western Nevada, 1961 and April 1962: Prepared for the Air Force Tech. Appl. Center, SRI, Proj. PHU-3678, Tech. Rept. No. 9.

White, D. E., 1969, Rapid heat-flow surveying of geothermal areas, utilizing individual snowfalls as calorimeters: J. Geophys. Res., v. 74, p.5191-5201.

Zbur, R. T., 1963, A geophysical investigation of Indian Wells Valley, California: U. S. Naval Ordinance Testing Station, China Lake, California, NOTS TP 2795, 98 pp.

APPENDIX I

Temperature-depth curves for the seven heat flow boreholes that were deep enough to provide a reasonable estimate of the geothermal gradient are presented in Figures I-1 through I-7. After the drilling and coring were completed, PVC pipe with a closure on both ends was lowered into the holes. Drill cuttings were caved around the pipe. The pipe was then filled with water in order to provide for thermal stability during future temperature measurements. All of the boreholes were completed above the local water table. Temperatures as a function of depth for each borehole are tabulated in Appendix II. Thermal conductivities as functions of depth interval are tabulated in Appendix III.

The temperature measurements in each of the boreholes are undisturbed and indicate conductive heat transfer in the shallow subsurface. Because of the high geothermal gradients, surface thermal effects are rapidly overcome. The one exception is the UTD-Coso #10 borehole with a gradient of 84°C/km and a temperature reversal between 5 and 15 meters caused by surface thermal effects. The boreholes are quite shallow (<100 m). However, with extrapolation of the shallow gradients to the surface, a surface temperature of approximately 20°C is predicted in good agreement with the mean annual surface temperature of approximately 19°C for the area.

Temperature-depth curves were not plotted for three of the boreholes, UTD-Coso #3, #4, and #9, because none of these holes penetrated deeper than 15 meters. Results from these boreholes, as well as from the other seven, indicate that the temperature data above 15 meters is useless for obtaining the geothermal gradient.

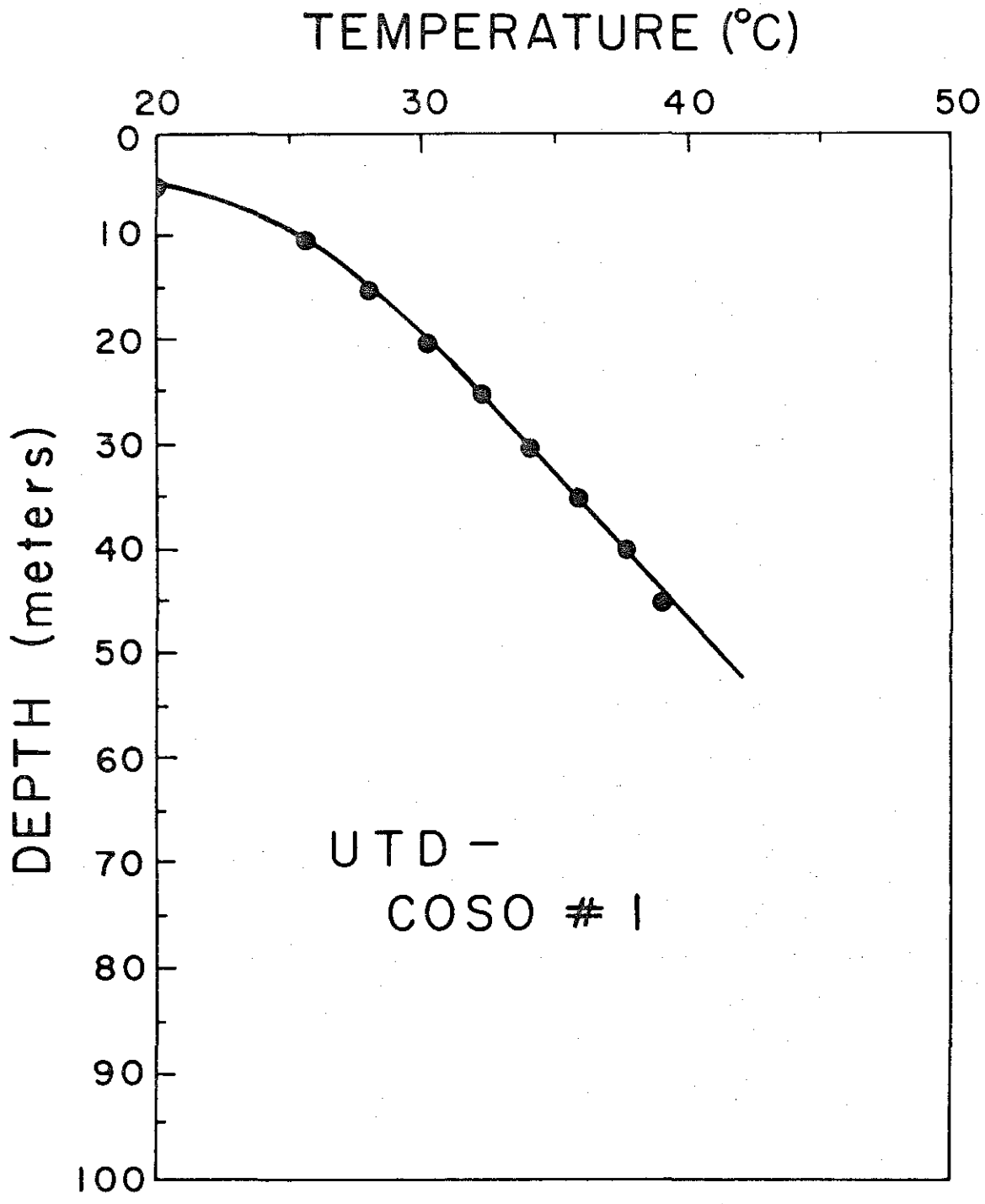

Figure I-1. Temperature-Depth Curve for Borehole UTD-Coso #1.

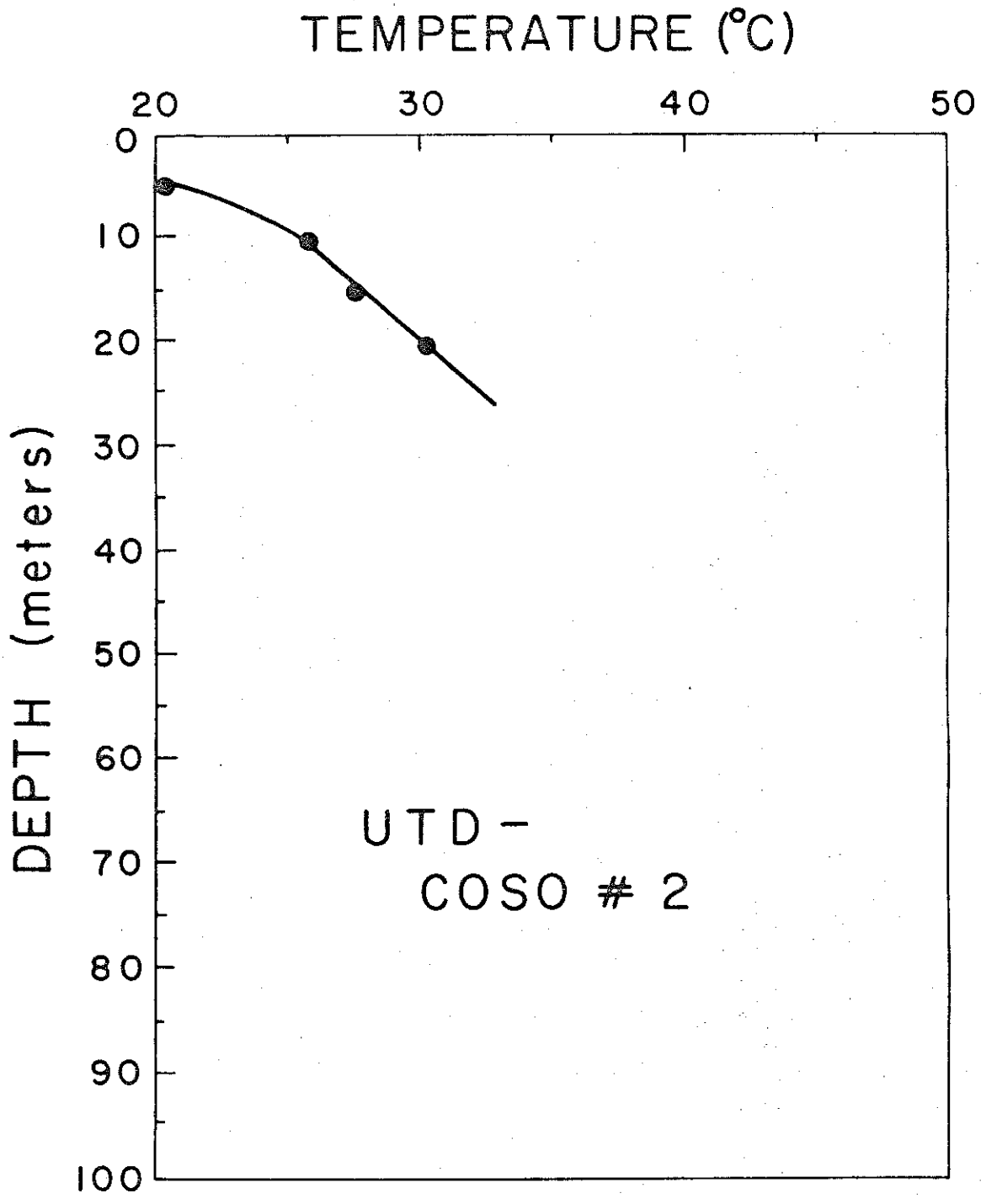

Figure I-2. Temperature-Depth Curve for Borehole UTD-Coso #2.

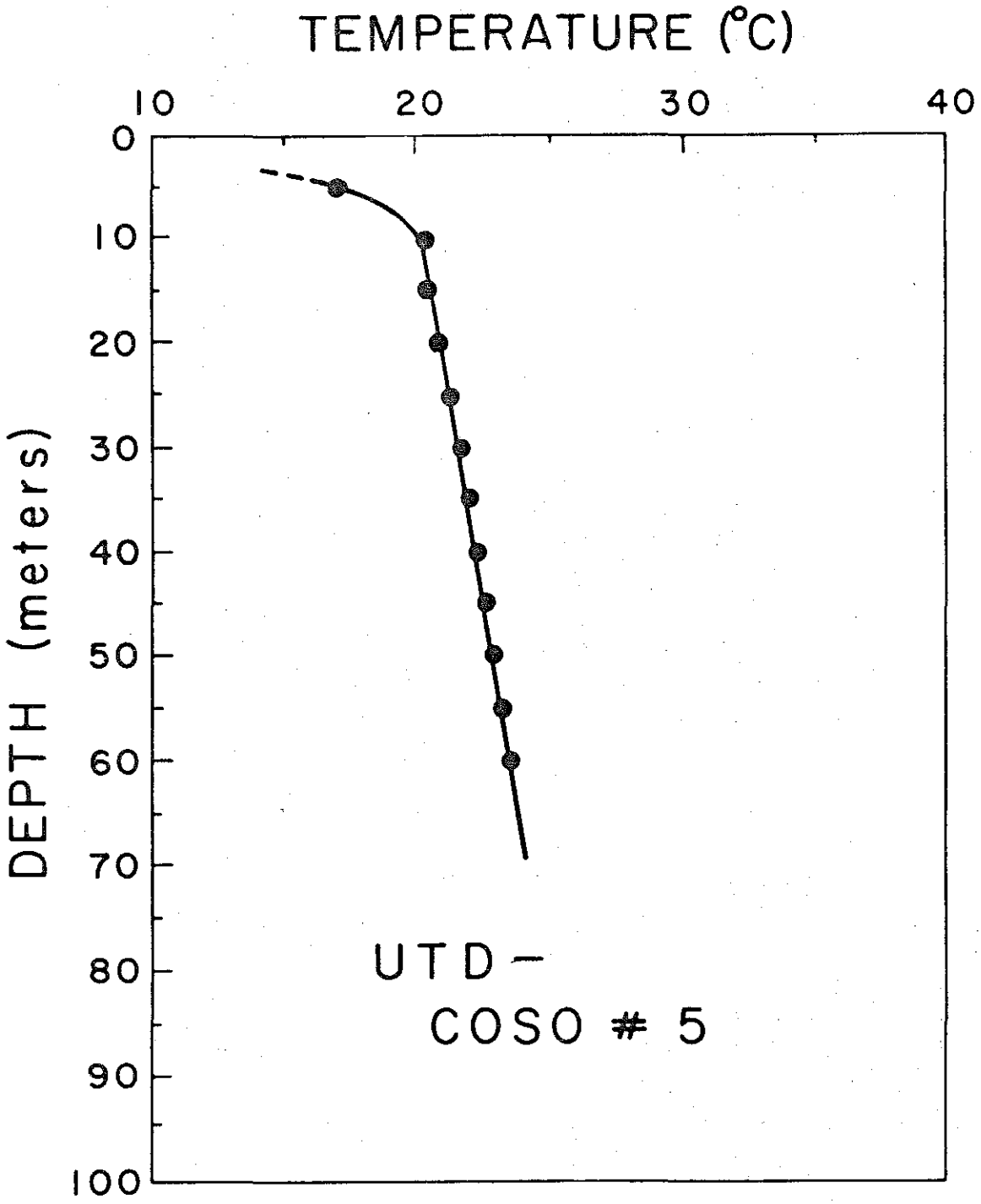

Figure I-3. Temperature-Depth Curve for Borehole UTD-Coso #5.

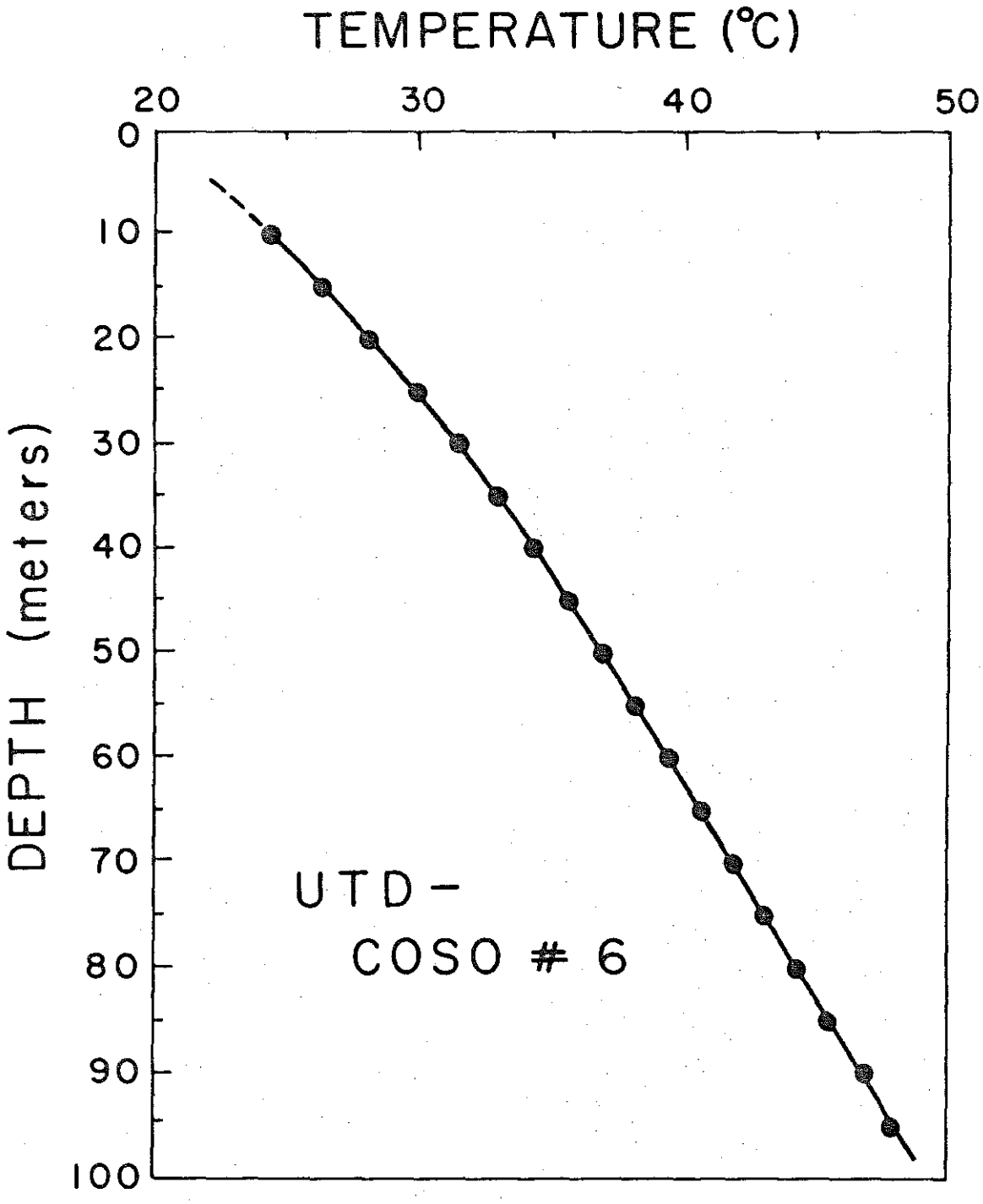

Figure I-4. Temperature-Depth Curve for Borehole UTD-Coso #6.

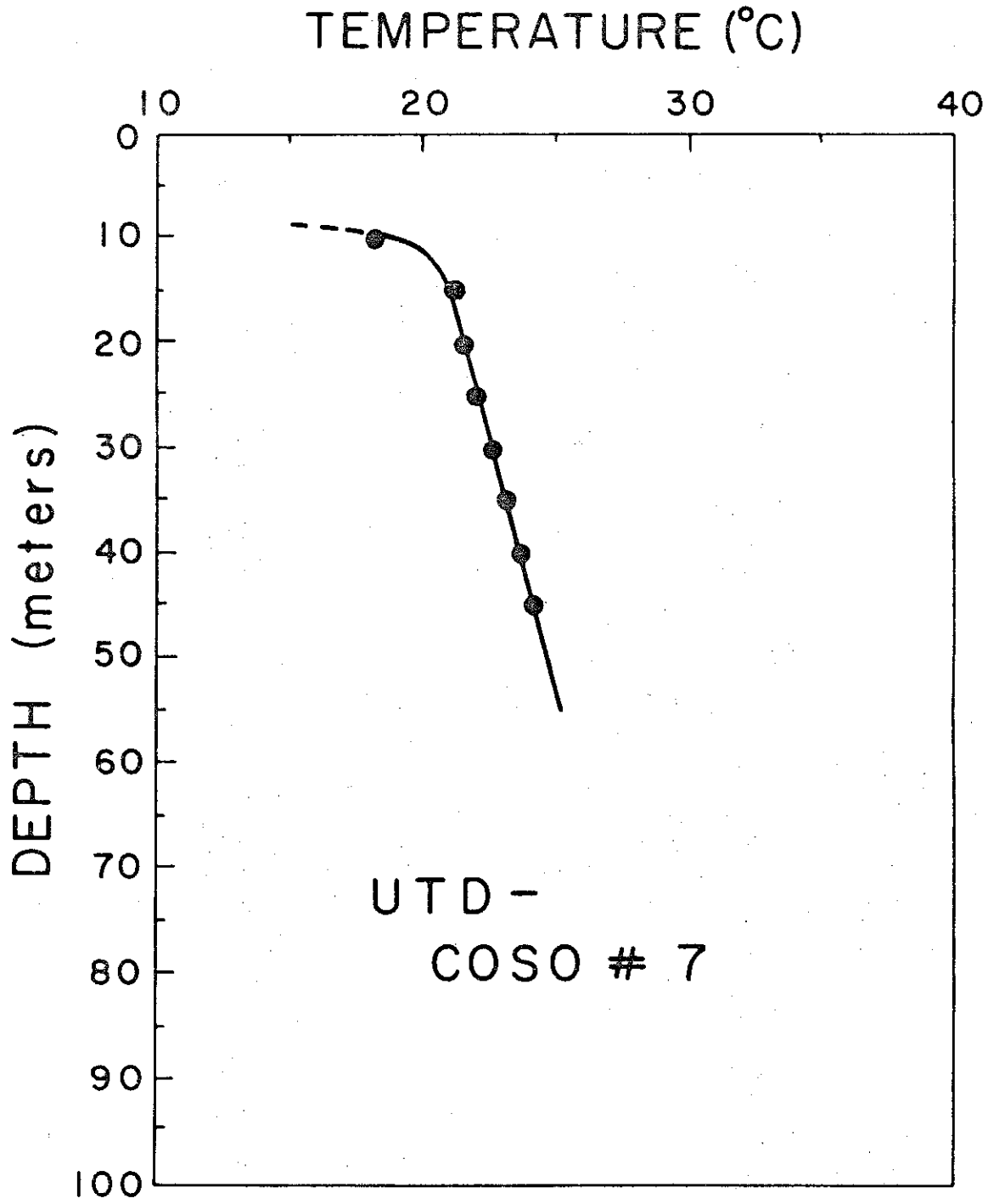

Figure I-5. Temperature-Depth Curve for Borehole UTD-Coso #7.

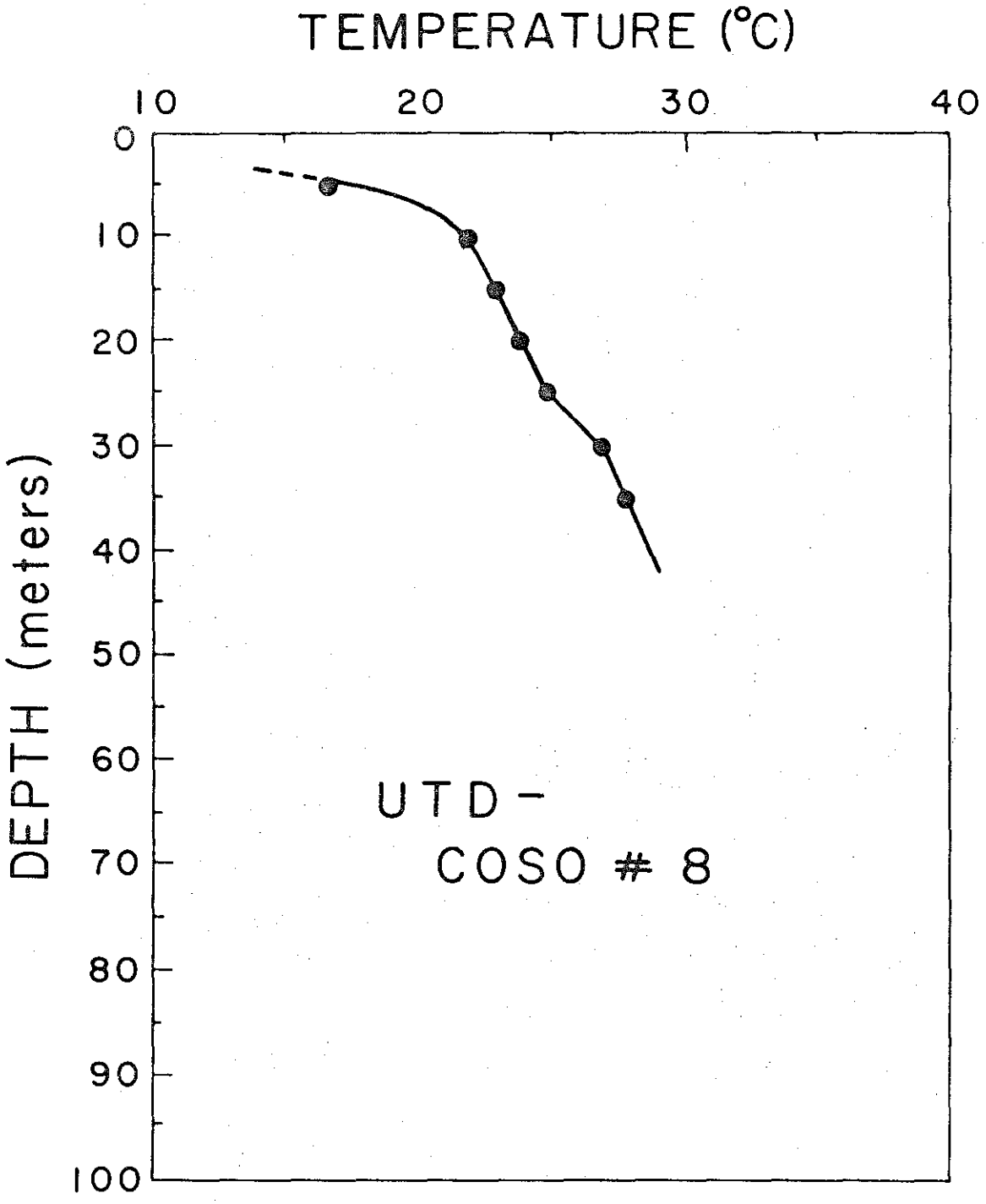

Figure I-6. Temperature-Depth Curve for Borehole UTD-Coso #8.

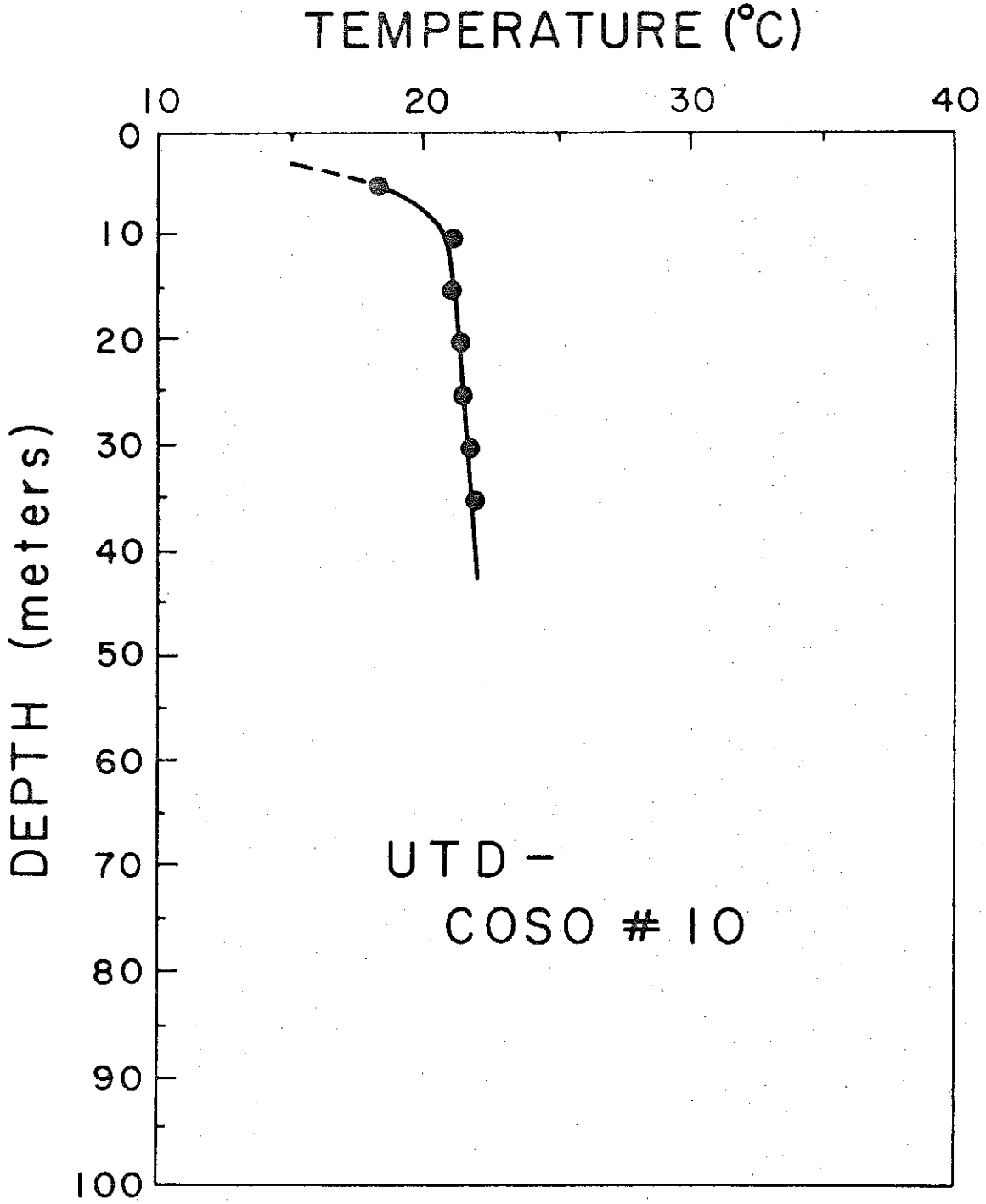

Figure I-7. Temperature-Depth Curve for Borehole UTD-Coso #10.

APPENDIX II

Temperature Measurements

In this appendix DEPTH refers to the depth in meters below ground level and TEMPERATURE is the temperature at the indicated depth in degrees Celsius.

UTD - Coso #1

Temperatures measured: 2/11/75

DEPTH	TEMPERATURE
0	11.12
5	19.61
10	25.60
15	27.96
20	30.21
25	32.22
30	34.03
35	35.82
40	37.62
45	38.94

UTD - Coso #2

Temperatures measured: 2/11/75

DEPTH	TEMPERATURE
0	9.70
5	20.29
10	25.75
15	27.56
20	30.30

UTD - Coso #3

Temperatures measured: 2/11/75

DEPTH	TEMPERATURE
0	7.47
5	12.29
10	15.89
15	15.77

UTD - Coso #4

Borehole too shallow for temperature measurements.
No data.

UTD - Coso #5

Temperatures measured: 2/11/75

DEPTH	TEMPERATURE
0	9.51
5	17.06
10	20.35
15	20.46
20	20.85
25	21.27
30	21.67
35	22.02
40	22.34
45	22.66
50	22.98
55	23.30
60	23.59

UTD - Coso #6

Temperatures measured: 2/10/75

DEPTH	TEMPERATURE
0	13.44
5	20.47
10	24.51
15	26.37
20	28.18
25	30.01
30	31.59
35	33.12
40	34.40
45	35.73
50	37.06
55	38.30
60	39.54
65	40.83
70	42.05
75	43.29
80	44.50
85	45.72
90	47.04
95	48.14

UTD - Coso #7

Temperatures measured: 2/10/75

DEPTH	TEMPERATURE
0	15.57
5	17.23
10	21.18
15	21.23
20	21.54
25	21.97
30	22.50
35	23.07
40	23.58
45	24.04
50	24.42

UTD - Coso #8

Temperatures measured: 2/11/75

DEPTH	TEMPERATURE
0	9.68
5	16.61
10	21.84
15	22.90
20	23.79
25	24.81
30	25.81
35	26.68

UTD - Coso #9

Temperatures measured: 2/11/75

DEPTH	TEMPERATURE
0	9.58
5	14.96
10	17.20

UTD - Coso #10

Temperatures measured: 2/11/75

DEPTH	TEMPERATURE
0	11.94
5	18.21
10	21.06
15	21.04
20	21.26
25	21.46
30	21.69
35	21.89

APPENDIX III

Thermal Conductivity Measurements

In this appendix DEPTH INTERVAL refers to the depth interval in meters below ground level from where the samples were collected and THERMAL CONDUCTIVITY is the thermal conductivity of the rock samples in units of 10^{-3}cal/(cm-sec-°C).

UTD-Coso #1

DEPTH INTERVAL	THERMAL CONDUCTIVITY
9-12	5.4
12-15	4.6
18-21	4.3
24-27	4.5
24-27	5.1
28-29	5.4
29-30	4.6
34-37	6,2
40-43	4.6
46-49	4.7

UTD-Coso #2

Borehole too shallow. No thermal conductivity measurements made. Value assumed corresponding to local geology.

UTD-Coso #3

Borehole too shallow. No thermal conductivity measurements made.

UTD-Coso #4

Borehole too shallow. No thermal conductivity measurements made.

UTD-Coso #5

DEPTH INTERVAL	THERMAL CONDUCTIVITY
3-6	5.3
6-9	5.1
9-12	4.6
15-18	4.8
21-24	4.8
27-30	5.1
27-30	5.3
34-37	4.6
40-43	5.4
46-49	5.3
52-56	5.3
58-61	5.0

UTD-Coso #6

DEPTH INTERVAL	THERMAL CONDUCTIVITY
0-3	5.5
3-6	5.1
6-9	5.0

UTD-Coso #6 (Continued)

DEPTH INTERVAL	THERMAL CONDUCTIVITY
9-12	5.2
15-18	5.4
18-21	4.9
21-24	5.3
27-31	5.2
31-34	6.8
34-37	5.1
37-40	5.0
40-41	5.0
40-43	4.8
43-46	4.9
46-49	5.5
49-52	5.8
52-55	4.8
55-58	5.5
58-61	5.4
61-64	5.2
64-67	5.9
67-70	5.6
70-73	5.1
73-76	4.5
76-79	5.0
79-82	5.2
82-85	5.4

UTD-Coso #6 (Continued)

DEPTH INTERVAL	THERMAL CONDUCTIVITY
86-87	5.5
85-88	5.7
88-91	5.3
91-94	5.6
94-96	5.1

UTD-Coso #7

DEPTH INTERVAL	THERMAL CONDUCTIVITY
15-18	6.5
18-21	6.7
21-24	6.3
27-30	5.2
27-30	5.1
34-37	6.5
40-43	6.9
46-49	6.4

UTD-Coso #8

DEPTH INTERVAL	THERMAL CONDUCTIVITY
9-12	7.2
15-18	5.6
21-24	4.7
27-30	6.8
34-37	6.4
40-43	7.0

UTD-Coso #9

Borehole too shallow. No thermal conductivity measurements made.

UTD-Coso #10

DEPTH INTERVAL	THERMAL CONDUCTIVITY
0-3	3.5
3-6	3.8
6-9	3.6
9-12	4.6
12-15	4.8
16-17	4.9
18-21	4.9
24-27	4.7
27-30	4.3